Stockholm University

# Studies of molecular clouds at the Galactic centre

Roland Karlsson

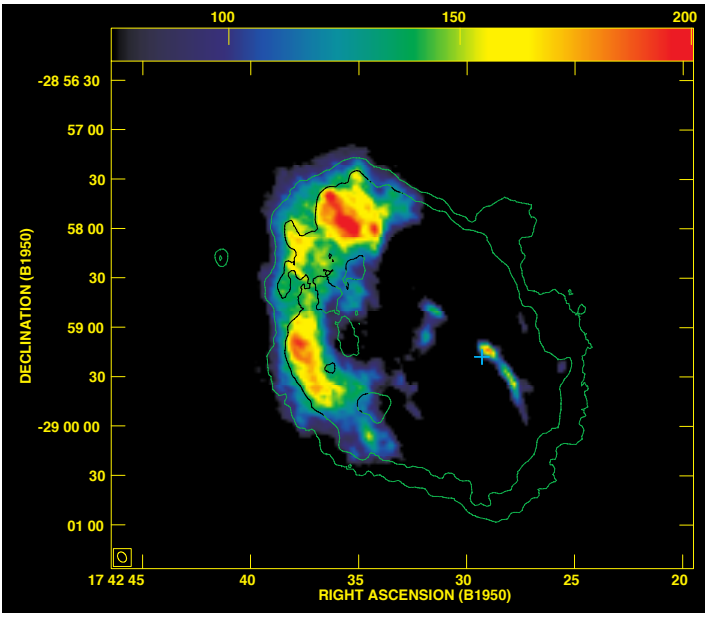

**Cover image:** Hydroxyl absorption at 50 $\mathrm{km\,s^{-1}}$ towards the Sagittarius A complex, showing the prominent +50 $\mathrm{km\,s^{-1}}$ cloud, and the OH-streamer that was detected by this work. Observations were made with the Karl Jansky Very Large Array, in Socorro, NM, USA. The location of the Galactic centre is marked with a plus sign, and the image covers a region of $\sim 10$ parsec from the centre with an angular resolution of about 7 arcseconds.

# Abstract

Interstellar molecular clouds play an essential role in the Universe. Such clouds are invoked for the production and destruction of stars, galaxies and gas and also for energy transport in galaxies. The Galaxy, or the Milky Way, is a large spiral galaxy, with a central bar structure, that harbours a few hundred billion stars and large amounts of gas and dust. At the centre of the Galaxy, a 4 million solar mass supermassive black hole resides, surrounded by a dense core of millions of stars, as well as molecular and dust clouds. The Galactic centre (GC) is hidden by gas and dust, such that only astronomical observations of radio-, infrared-, X-rays and gamma-rays are available for a gathering of information at the centre. In this work, I have studied neutral molecular clouds in absorption at the innermost 50 light years from the centre with the Karl Jansky Very Large Array Observatory in New Mexico in the USA, and with data from observations with the Swedish-ESO Submillimetre Telescope in Chile, and also from the orbital observatory *Odin*. I have detected a new stream-like feature of gas that seems to link a previously known ring of gas clouds (the CND) and the GC. Moreover, the hypothesis of feeding the CND from an outside cloud is supported by this work. Contemporary discussions in the literature that the central bar structure would act as a pump of material inwards from the spiral arms towards the GC via molecular clouds are also suggested by the data. A number of maser sources have been observed and some of those are shown to reside at shock fronts or anticipated regions of collisions between molecular clouds or at star forming regions. Unusually high water abundance was detected at the southwest part of the CND, indicative of shocks and strong turbulence. Moreover, I have produced high-resolution spectral line maps of hydroxyl (OH) absorption intensity in the four main transition lines of OH at 1612, 1720, 1665 and 1667 MHz, as well as apparent opacity and position-velocity maps of the GC region.



ISBN 978-91-7649-356-4

Department of Astronomy, Stockholm University

*This thesis is dedicated to my beloved wife,*
*Marianne*

# List of Papers

The following papers, referred to in the text by their Roman numerals, are included in this thesis.

## Publications included

**PAPER I: 18-cm VLA observations of OH towards the Galactic Centre**
Karlsson, R., Sjouwerman, L. O., Sandqvist, Aa., Whiteoak, J. B. 2003, A&A, 403, 1011

**PAPER II: Hydroxyl, water, ammonia, carbon monoxide and neutral carbon towards the Sagittarius A complex. VLA, *Odin*, and SEST observations**
Karlsson, R., Sandqvist, Aa., Hjalmarson, Å., Winnberg, A., Fathi, K., Frisk, U., Olberg, M. 2013, A&A, 554, 141

**PAPER III: The OH-streamer in Sagittarius A revisited: analysis of hydroxyl absorption within 10 pc from the Galactic centre.**
Karlsson, R., Sandqvist, Aa., Fathi, K., Martín, S. 2015, A&A, 582, A118

## Publications not included in this thesis

**PAPER IV: The 18 cm OH distribution in the Galactic Center Torus**
Sandqvist, Aa., Karlsson, R., Whiteoak, J. B., & Gardner, F., F. 1987, AIP Conf. Proc. 155, 95: ed. D.C. Backer (AIP, New York)

**PAPER V: OH in the environment of Sgr A**
Sandqvist, Aa., Karlsson, R., & Whiteoak, J. B. 1989, IAU Symp 136, 421: ed. M. Morris (Kluwer, Dordrecht)

**PAPER VI: Absorption and Emission in the Four Ground-State OH Lines Observed at 18 cm with the VLA Towards the Galactic Centre**
Karlsson, R., Sandqvist, Aa., Sjouwerman, L. O., & Whiteoak, J. B. 2003, Astronomische Nachrichten Suppl. Issue 1, 324, 223

**PAPER VII: Hydroxyl, water, ammonia, carbon monoxide, and neutral carbon towards the Sgr A complex.** Karlsson, R., Sandqvist, Aa., Hjalmarson, Å., Winnberg, A., Fathi, K., Frisk, U., Olberg, M. 2013, IAUS, 303, 97

**PAPER VIII: The gravitational potential of NGC 1097 and inward migration of the circumnuclear ring.** Piñol-Ferrer, N., Fathi, K., Font, J., Karlsson, R., Hernandez, O., van de Ven, G., Carignan, C. 2014, MNRAS, 438, 971

**PAPER IX: VizieR Online Data Catalog: OH-streamer in SgrA at 1665 and 1667MHz (Karlsson+, 2015)** Karlsson, R., Sandqvist, Aa., Fathi, K., Martín, S., 2015yCat..35820118

# Author's contribution

PAPER I: I contributed to the preparation of the proposal to NRAO, as well as the full procedure for preparing and performing the observations, together with Aage Sandqvist, John Whiteoak and Frank Gardner. The post-observational calibration of the data was made at the VLA together with Aage Sandqvist. The processing of the calibrated data was made mainly by myself, as well as the production of most figures in the paper. The planning, preparation and performing of the second observation run at the VLA site (including full data calibration and analysis), were fully my responsibilities. The OH maser parts in the paper were made by Lorant Sjouwerman, while the analysis and conclusions were performed together with the co-authors.

PAPER II: I made all the processing and calibration of the OH data. The calibrated SEST data were available from Aage Sandqvist, and my contribution was to produce the CO maps, calculations and analyses. I participated in preparing the observational file for the *Odin* observations from 2011 and on. Analysis and conclusions in the paper were, to a major part, on me.

PAPER III: I produced the intensity-, $-T_{\rm L}/T_{\rm C}$ and position-velocity maps, as well as the calculations of opacities and column densities. The analysis and conclusions about relative positions and interactions of observed features were also on me. Furthermore, I stand behind the ideas of interaction between the OH-streamer and CN clumps and the blobs of weak radio emission projected inside of the OH-streamer.

# Contents

# 1. Introduction

## 1.1 Thesis project

This thesis is based on radio astronomical observations and presents an analysis of the morphology and kinematical behaviour of selected neutral molecular gas clouds in the central parts of the Galaxy (the Milky Way). In Chapter 1 a brief motivation for the work is presented. Chapter 2 contains a review of the Galaxy and its central region, to shed light on possible links between the large and small scale happenings in the Galaxy, which are addressed in this thesis. Some of the results are also included at relevant places in this chapter. Chapter 3 explains the utility and strength of radio astronomical observations in general. Chapter 4 is a summary of the papers included in this thesis, while Chapter 5 contains some ideas of continued research on the OH-streamer and the 3D structure in the 10 pc vicinity of the Galactic centre.

The aim was to study morphology, kinematics and hierarchy of some previously known molecular clouds in absorption at high angular and velocity resolutions at the inner parts of the Galaxy. Observations were made towards the Galactic centre (GC) mainly of the hydroxyl radical (OH) but also of other molecular species, both in absorption and emission. The vast majority of data comes from absorption measurements of OH with the Karl G. Jansky [1] Very Large Array (VLA), which provided supreme angular resolution and sensitivity. Also, data from the Swedish-ESO Submillimetre Telescope (SEST) and the *Odin* satellite observatory have been used for investigations of the carbon monoxide and water species, with high velocity resolution, but less angular resolution compared to the VLA. The *Odin* satellite has provided a long time series of water observations. The main region studied in this work covers the inner ten pc from the dynamical centre of the Galaxy, which comprises a range of objects, such as neutral and ionised atomic and molecular clouds, dust, and stars. In this work, only neutral molecular clouds are studied, and although those may be partly ionised on the surface, we do not consider magnetohydrodynamic effects to be dominant over gravitational and fluid dynamical forces.

[1] The "father of radio astronomy", who already in 1931 was able to identify radio signals from space (in fact peaking towards the Galactic centre) during his investigation of disturbances in "short wave" (wavelength 14.5 meter) radio communication.

Observation of molecular clouds may give information about formation and evolution of star-forming complexes, ignition of starbursts as well as the overall kinematic behaviour of the interstellar medium throughout the Galaxy. In spiral galaxies, radial transport of material is considered essential for the build-up of the energy budget and the evolution of the various phenomena that are observed at different galactocentric radii.

In barred spiral galaxies like the Galaxy, large scale transversal bars are suggested to pump material inwards such that the centre region is supplied with gas, dust and stars. Some of that material may travel towards the very centre of the Galaxy and ultimately feed the elusive central supermassive black hole (SMBH). The existence of an SMBH at the centre now appears to be concluded by precision measurements of star motions near the dynamical centre of the Galaxy. An extremely compact non-thermal strong, moderately variable, radio source, Sagittarius A$^\star$ (Sgr A$^\star$), appears to be colocated with the SMBH.

In the ten pc regions from the GC, we have observed some of the large previously known molecular clouds (e.g. the +20 (GMC M-0.13-0.08) and +50 (GMC M-0.02-0.07) and +80 km s$^{-1}$ clouds), and the circumnuclear disk (CND) which in fact is a collection of clumps in systematic rotation about the GC. The CND is likely to be replenished by the +20 km s$^{-1}$ cloud via an object at the north tip of the +20 km s$^{-1}$ cloud, the Southern streamer, and possibly also by other streamers. A new feature was detected by this work, a clumpy object that we call the OH-streamer, which also seems to transport material towards the GC.

The results in this thesis support the scenario of the CND being fed by the +20 km s$^{-1}$ cloud located south of the GC. We also argue that the OH-streamer is a stream of gas that connects the CND and a region in the 0.1 pc scale vicinity of the SMBH. A relation between the OH-streamer and an adjacent molecular cloud, the +80 km s$^{-1}$ cloud is also found, and we interpret our high spatial and velocity resolution data as these two features are interacting. In this study, we also consider that the main parts of the OH-streamer are transient features, which would imply a non-continuous feeding of OH towards the SMBH. The OH-streamer may, however, not be the sole source of material transfer into the nucleus, but other streamers, *viz*. the Northern streamer, would also feed the nucleus. The observed transfer rate of matter in streamers is, however, extremely low compared to what is expected for feeding of an active galactic nucleus, but some of the observed short time scale variations of radio emission from Sgr A$^\star$ could be explained by a repetitive inflow of material from streamers.

With the VLA, the kinematics of large molecular clouds at the GC can be studied at unprecedented angular- and velocity resolution, such that we were able to suggest a physical interactions between some of the objects based on

the position-velocity maps of OH absorption. Subsequent comparison of the OH absorption with emission line observations of other molecules (e.g. $C^{18}O$ in $J = 2 - 1$) also helped to unravel the morphology of some molecular and continuum components. Observations of a few other molecular species, both in absorption and emission, towards the GC region shed even more light on some of the objects observed in OH absorption. Moreover, we have produced a catalogue of high-resolution absorption and apparent opacity maps of OH in the GC region in the energy transitions of the main transition lines at 1665 and 1667 MHz, as well as absorption maps in the satellite lines at 1612 and 1720 MHz.

# 2. The Galaxy and the Galactic centre

Galaxies appear projected on the sky in a wide range of morphological characteristics, and several classifications of galaxies have been suggested. In the late 1920s, the American astronomer Edwin Hubble developed a scheme that is still in use, the Hubble tuning fork diagram. The main Hubble classes are ellipticals (E), spirals (S) with and without bars, and irregulars (Irr). Morphologically, a spiral galaxy comprises a thin disk with spiral arms containing stars, gas and dust and a dense central bulge of stars. In some cases, a transverse central bar (or bars) structure is observed, which is denoted by a B as second letter. The main classes are further divided into subclasses. For spiral galaxies, commonly a lower case letter is added to denote the character of the winding of the spiral arms. However, intermediate classes also occur. A so-called grand design spiral galaxy is one where the spiral arms are well-defined. It is generally assumed that a central supermassive black hole (SMBH) resides at the dynamical centre of most spiral galaxies. Galaxies are observed to be gravitationally bound to other galaxies in groups or clusters of galaxies. The two galaxies nearest to the Galaxy are the Magellanic clouds, located at about 160 000 light years from the Galaxy.

## 2.1 The Galaxy — the Milky Way spiral galaxy

The Galaxy, in which our solar system resides, is a large spiral galaxy containing an estimated number of about 200 billion stars and was formed a few hundred million years after the anticipated Big Bang (e.g. Churchwell et al. (2009)). The Galaxy belongs to the Local Group of some 30 galaxies while the observable Universe comprises an estimated number of $10^{11}$ galaxies. The Galaxy hosts a central bar structure and is classified as an SBb or SBc galaxy, i.e. a barred spiral galaxy with loosely wound spiral arms. The basic structure is two spiral arms. However, there are traces of smaller arm-like features, and also, more than one central bar may exist. The diameter is about 100 000 light years, $\sim$ 35 kiloparsec (kpc), and the average thickness of the disk is about $\sim$ 0.3 kpc (Fig.2.1). To explain the observed dynamical characteristics of the

Galaxy, it is suggested that a halo is surrounding it. Calculations have shown that about 90 % of the mass of the Galaxy is hidden in a halo composed of the so-called dark matter. The virial mass, i.e. a reasonable measure of the mass, of the Galaxy including the dark matter, is estimated to be about $1.3 \times 10^{12}$ $M_{\odot}$ (McMillan (2011)). Different values of the distance from the Sun to the GC are given in the literature, ranging from about 7.5 to 8.5 kpc. Gillessen et al. (2009) use e.g. 8.33 $\pm$0.35 kpc (about 27 000 light years). However, we use 8 kpc for consistency with previous work. Estimates of the mass of the SMBH are dependent on the distance to the GC. The rotation period of the Sun about the centre is about 200 M years while the bar has a shorter rotation period. The Galaxy is considered to have an active galactic nucleus (AGN), but at the present epoch, the nucleus seems to be in a quiescent state. Repeated activity is, however, observed at the centre, where the compact radio source Sgr A* is located. The radio emission from Sgr A* is observed to vary significantly on timescales as small as hours, and the variations are taken as signs of infall of matter towards the SMBH. Gas clouds captured in the gravitational field and stellar winds may feed accretion disks surrounding the SMBH, and ultimately material may fall in towards the SMBH and give rise to bursts of radio and X-ray emission from Sgr A*. The accretion rate is extremely low, on the average only about a few $\times 10^{-6}$ $M_{\odot}$ per year, let it be only from stellar winds (Cuadra et al. (2005) and (2006)).

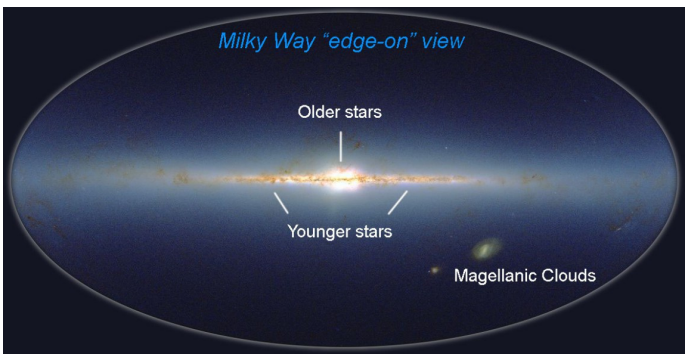


**Figure 2.1:** Mosaic obtained as part of the Two Micron All Sky Survey (2MASS), a joint project of the University of Massachusetts and the Infrared Processing and Analysis Center/California Institute of Technology, funded by the National Aeronautics and Space Administration and the National Science Foundation).

The baryonic matter (ordinary matter) in the Galaxy is bound in some $10^{11}$ stars and in large amounts of gas and dust. Star formation is active in the spiral arms and at the centre. The density of stars varies significantly in the Galaxy.

In the central region, star densities of up to $10^7$ $M_\odot pc^{-3}$ are found, but is only about 0.05 $M_\odot pc^{-3}$ in the vicinity of the Sun. About half of the mass of the interstellar medium in the Galaxy, about $(2-4) \times 10^9$ $M_\odot$, is in the form of gas in molecular clouds. The mass inside of the orbit of the Sun about the centre is calculated to be about $10^{11}$ $M_\odot$.

Stars in the Galactic disk orbit the GC in the same direction as the spiral pattern, and essentially in the same plane. However, due to the gravitational field of the disk, the stars wobble up and down through the nominal plane of the disk on a timescale of about 70 M years.

### 2.1.1 The Galactic halo

In the spheroidal Galactic halo, old ($(10-13) \times 10^9$ years)) and low-mass, mostly red, (so-called Population II) stars move in randomly oriented orbits. Those stars contain essentially only hydrogen and helium. There are very little gas and dust in the halo, and star formation stopped a long time ago. The number of halo stars is about 20 % of the number of disk stars. The Population II stars in the halo have higher velocities relative to the Sun than the Population I of hot and young stars, residing in the disk. In the halo, the globular clusters of stars are found. Globular clusters are dense balls of $10^5 - 10^6$ stars with ages of a few $10^9$ years. About 1% of the stars in the halo are bound in the globular clusters, where the matter density may reach $10^4$ $M_\odot pc^{-3}$. The Galactic halo is also considered to contain most of the dark matter.

A scenario of formation of the Galaxy suggests that gas with low angular momentum has collapsed into the halo and into the embryo of the central bulge. The central bulge stars orbit the centre in randomly oriented elliptical orbits and contain various amounts of elements heavier than hydrogen and helium (metals in Astronomy). The remaining gas with higher angular momentum then collapsed into the formation of the Galactic disk, where star formation began as a result of cloud-cloud collisions (e.g. Mo et al. (1998)). The halo is suggested to still feed the central parts of the disk with low metallicity gas (Morris & Serabyn (1996)), and the halo itself may be fed by streams from the Large and Small Magellanic clouds (Nidever et al. (2010), Fig. 2.2).

### 2.1.2 Bar(s) and spiral arms in the Galaxy

It is not trivial to reveal the structure of the Galaxy from the Sun's position inside of the Galaxy. Models of the Galaxy are built by observing neutral hydrogen, star formation regions and young stars and plotting their distances, directions and velocities relative to the Sun. It is found that star formation regions and young stars are concentrated in bands, both towards and away from

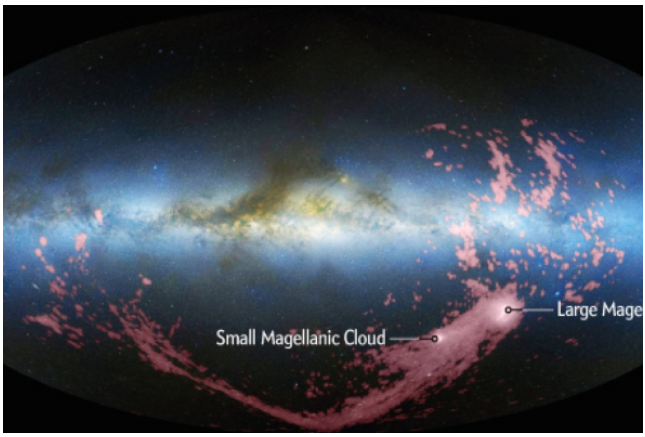


**Figure 2.2:** Image of the Galaxy observed in neutral hydrogen (H I). The white band delineates the Galactic disk, and the pink clouds are streams of gas that connect the Large and Small Magellanic clouds galaxies and are suggested to also feed the Galactic halo with gas (Nidever et al. (2010)), reprinted by permission of the AAS).

the Galactic centre, which is indicative of the existence of spiral arms. Figure 2.3 is an artist's view of how the Galaxy would look like from above.

A rotation diagram, rotation velocity versus distance from the centre, may be used to find out what kind of rotation that prevails in the Galaxy. If the prevailing rotation was purely Keplerian, the rotation velocity, $V_c$, would fall off as the square root of the radius ($R$), i.e. $V_c(R) \propto R^{-1/2}$, which neither is observed in the Galaxy nor in other spiral galaxies. However, regions of Keplerian motions occur at certain radii.

The rotation characteristics of the Galaxy are complex and comprise the sum of contributions from bulge and disk stars, gas and the spheroidal halo. The observed rotation curve of the Galaxy may be described as solid body rotation out to about 0.5 kpc and Keplerian rotation from 0.5 kpc to about 3 kpc while the rotational velocity increases between $\sim 3 - 7$ kpc. In the neighbourhood of the Sun, another Keplerian-like velocity decline is observed. At greater distances, outside of the orbit of the Sun, the rotation curve flattens out. The marked deviance from Keplerian rotation outside of the Sun is a strong argument for the existence of a spheroidal halo of dark matter. However, it should be noted that observations outside of the Sun's orbit have substantial uncertainties (Fig. 2.4). The intricate rotation features of the Galaxy result in differential rotation such that disk stars and any additional pattern residing in the disk (e.g. bar(s) and spiral arms) may have different rotation velocities

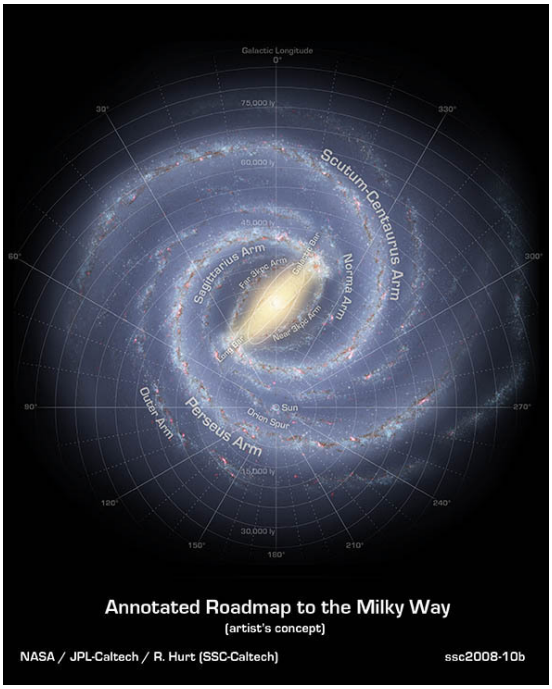


**Figure 2.3:** Artist's conception of the Milky Way galaxy as seen from the Galactic North pole. The commonly used names of the spiral arms are shown, as well as the central bar structure. Note the position of the Sun at the centre of the coordinate system (Courtesy NASA/JPL-Caltech/R. Hurt SSC/Caltech).

at different radii. This inequality of rotation forces interstellar gas clouds and stars to move in and out of the arms depending on where they are with respect to the Galactic centre.

The presence of a central bar was first suggested to account for the observed non-circular motions of H I near the Galactic centre by de Vaucouleurs (1964) and Peters (1975). Liszt & Burton (1980) discussed the morphology of a central bar structure within about 2 kpc, that is tilted about 24° from the rotation axis of the Galaxy, based on H I data. Morris & Serabyn (1996) estimate the mass of the bar to be $(1-3)\times10^{10}$ $M_{\odot}$. It is suggested that central bars play a role in the migration of gas and stars towards the centre and feeding of central black holes in spiral galaxies (Shlosman (2012), and references therein).

Gerhard (2008) models a Galactic bar with a pattern speed of $52\pm10$ km s$^{-1}$ kpc$^{-1}$ (implying a bar corotation radius at 3.5 – 4.5 kpc), however, these parameters are much less rigorously constrained than for the Galactic

spiral arms. The spiral arm pattern in the Galaxy is likely rotating as a solid body with a pattern speed about one-third of the Galactic bar (e.g. Quillen & Minchev (2005)), which would imply that the main Galactic bar and the spiral arms are dynamically decoupled structures. It should, however, be noted that these results are still under scrutiny, and there is a body of works that questions the values stated here and even the number of bars in the Galactic disk (e.g. Cabrera-Lavers et al. (2006); Nishiyama et al. (2005) and Wegg et al. (2015)).

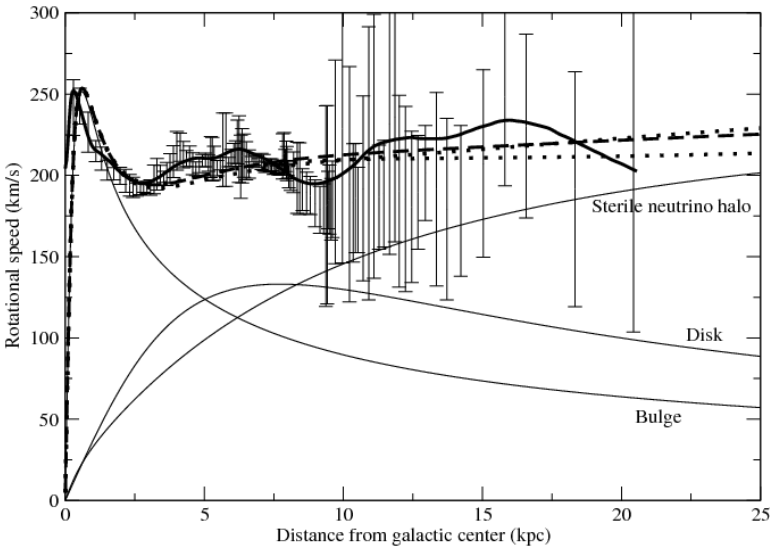


**Figure 2.4:** Observed and fitted rotation curve of the Galaxy. The solid dark curve is the observed data obtained by Sofue et al. (1999) and the error bars are the latest data obtained by Sofue (2011). The components of the sterile neutrino halo, the disk and bulge that contribute to the total rotation curve are also shown (Figure by Chan & Ehrlich (2014), Springer license number 3796420131061).

### 2.1.3 The interstellar medium

The interstellar medium (ISM), is the material between the stars in a galaxy. In the Galaxy, it is composed of about 90 % gas and 10 % of dust, but the particle density in the ISM is extremely low, only about 1 atom per $cm^3$. As a comparison, the atmosphere at sea level on the Earth comprises about $2 \times 10^{19}$ molecules per $cm^3$. Nevertheless, the ISM is responsible for absorption and scattering of visible light. The central parts of the Galaxy are obscured by a 30 magnitude absorption, meaning that only one of $10^{12}$ photons from the centre

reaches the Earth (Schlegel et al. (1998)). Optical observations of the centre are therefore ruled out. However, the inner parts can be observed at both shorter and longer wavelengths than the visual, and the vast majority of electromagnetic energy reaching us from the Galactic centre region comes from infrared radiation. The interstellar matter in the inner few hundreds of pc of the Galaxy is mainly molecular. The average density ($n_{H_2}$) in molecular clouds in this part of the Galaxy is $\sim 10^4$ molecules per cm$^3$ and the velocity dispersion is about 20 km s$^{-1}$ (Rodríguez-Fernandez & Martín-Pintado (2001)).

### 2.1.4 The Galactic disk

The Galactic disk is thin compared with its radius, generally less than 0.3 kpc at the Sun's position, while the radius of the disk is about 15 kpc. The disk contains gas, dust and Population I stars with high angular momentum, medium to high mass, and a metallicity of the same order as the Sun. The material in these younger stars has been subject to recycling by supernova events and are enriched with heavier elements compared to the metal-poor Population II of old stars in the halo. In the disk, there are also open star clusters with $10^2 - 10^3$ stars with ages less than $10^9$ years. The region between 0.5 to 3 kpc from the Galactic centre has a low content of gas (Fig. 2.5). However, the gas density increases rapidly from about 4 to 6 kpc, which may indicate the presence of one or more spiral arms in the region where the Scutum-Centaurus arm is seen in Fig. 2.3.

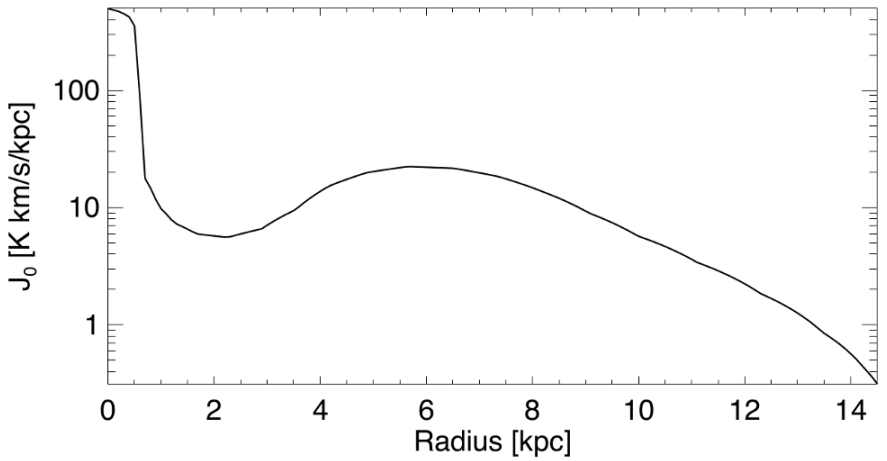


**Figure 2.5:** Azimuthally smoothed radial distribution of $^{12}$CO surface brightness in the Galaxy, derived from Bally (1989).

### 2.1.5 The central molecular zone

The central molecular zone (CMZ), is a giant complex of molecular clouds in a 0.3° wide band around the GC, between Galactic longitudes ($l$) of $-1.1°$ to 1.9°, and is about 300 pc wide (Fig. 2.6). The CMZ matches the size of the nuclear stellar bulge (a few 100 pc), where the star formation rate times the Hubble time ($t_{\rm Hubble}$) also matches the mass of the bulge ($M_{\rm bulge}$) (Morris & Serabyn (1996)). This is consistent with a continuos star formation over the life-time of the Galaxy. The CMZ contains $\sim 5\times10^7$ $M_\odot$ of molecular gas, i.e. $\sim$ 10 % of all gas in the Galaxy. The CMZ also includes the most massive star forming region in the Galaxy, Sgr B2, a giant molecular cloud located about 120 pc north-east of the centre. The initial mass function (IMF) of the CMZ is "top heavy", i.e. there is bias towards high mass stars.

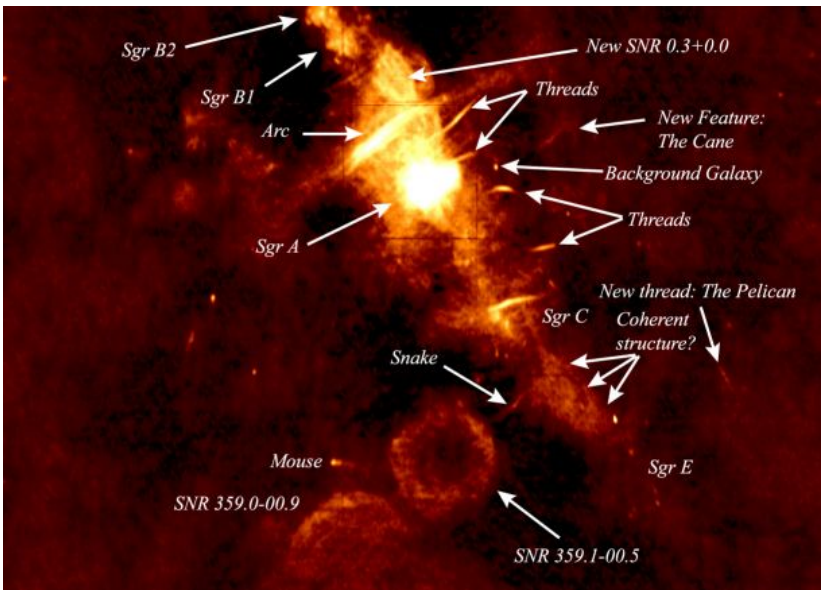


**Figure 2.6:** 90 cm (330 MHz) VLA radio image of the Galactic Centre covering a $2° \times 2°$ region of the CMZ at 45" angular resolution. It shows the most prominent features at centimetre wavelengths and is orientated as RA/Dec (Kassim, et al. (1999), by permission of the Astronomical Society of the Pacific Conference Series).

The GMCs in the CMZ are quite different from the "normal", less dense ($n \sim 10^3$ – $10^4$ cm$^{-3}$), molecular clouds in the spiral arms. Moreover, in the CMZ, the GMCs are rich in a large number of complex and rare, and even organic, molecules, e.g. $CH_3OH$ and HCOOH. The complex molecules are formed on dust grains, where shocks liberate them into the gas phase by sput-

tering, i.e. bombardment by energetic particles (Requena-Torres et al. (2006)). Supersonic shocks in the CMZ are also likely to be responsible for maser emission in cloud-cloud collisions associated with the expansion of supernova remnant (SNR) material, or in processes of star formation (Sjouwerman et al. (2010)).

The CMZ molecular clouds are relatively warm, 80 K on the average, but temperatures may locally reach up to 500 K. About 1/3 of the total gas column is at $150 - 200$ K (Morris (2010)). Such temperatures are much higher than that of the molecular gas in the disk (10–20 K) and require a strong heating source. Taking into account the significant cooling rate of abundant species such as $C^+$, CO and $H_2$, it is a challenge to find the heating source. Several candidates have been proposed for the heating e.g. low-velocity C-shocks from turbulent motions (Rodríguez-Fernandez et al. (2004), and references therein). Morris et al. (1983), discuss heating by starlight, cosmic ray heating and soft X-rays, but do not reach a conclusion of the heating source. However, shock heating of the gas and X-ray flashes may give rise to local temperature spikes that can speed up the evaporation of molecules from grain surfaces, and alter the chemistry of the interstellar medium. Both the higher temperatures and high-velocity dispersion in the CMZ favour formation of higher mass stars.

Comparatively, strong magnetic fields are observed in the CMZ dense molecular clouds and are generally aligned with the Galactic plane, and perpendicular to the plane in lower density clouds, (Fig. 2.7). The observed sample is, however, yet very small.

The distribution and kinematics of molecular clouds in the CMZ are inconsistent with both axial symmetry and uniform circular rotation about the GC (e.g. Jackson et al. (1993), and references therein). It is suggested that the large-scale bar structure of the Galaxy acts in pumping gas from the kpc scale to the hundreds of pc scale disk (Genzel & Poglitsch (1995) and Martinez-Valpuesta & Gerhard (2012)). The bar potential has a family of stable orbits, Fig. 2.8, and the gas is compressed at the cusps or intersecting tips of the inner orbits, loses energy and falls inwards to settle in an $X_2$ orbit. The compression and subsequent cooling may cause the gas clouds to transform from atomic to molecular form, according to Morris & Serabyn (1996).

The CO gas dynamics of the inner $\sim$10 kpc of the Galaxy is seen in the Galactic longitude-velocity diagram in Fig. 2.9. The complex velocity behaviour of the CMZ can be studied near 0 deg longitude. The 3-kpc arm is also indicated. The major red diagonal structure in the figure originates in the Norma and Scutum-Centaurus spiral arms (see Fig. 2.3).

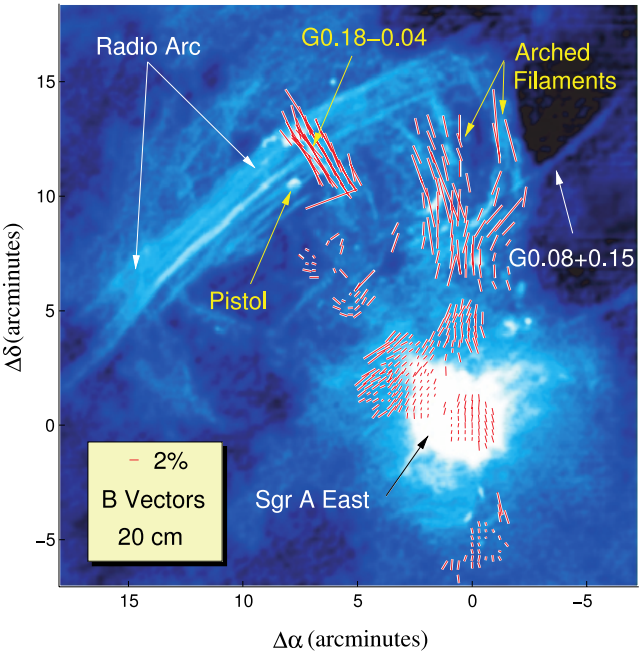


**Figure 2.7:** Magnetic field directions inferred from measurements of the orientation of the polarized E- vectors of thermal emission from magnetically aligned dust grains at a combination of far-IR and submm wavelengths from Chuss et al. (2003). The underlying VLA radiograph, from Yusef-Zadeh et al. (1984), shows 20 cm emission from a $60 \times 60$ pc region. The Galactic plane is oriented at a position angle of about $30^{\circ}$ east of north, and the Galactic centre is located within the radio bright Sgr A complex (Chuss et al. (2003), reprinted by permission of the AAS).

### 2.1.6 The expanding molecular ring

Observations by Bally et al. (1987) and (1988) of $^{13}$CO revealed a structure that seems to resemble a rotating ring of gas, the expanding molecular ring (EMR), or expanding molecular shell. The EMR is characterized by a $\sim 200$ pc ring, which exhibits both high positive and negative velocity features delineating an ellipse in the $(l, V)$ diagram (Scoville (1972); Kaifu et al. (1972) and (1974)). The shell is expanding at about 160 $\mathrm{km\,s^{-1}}$ and rotates at about 70 $\mathrm{km\,s^{-1}}$. The projected velocities of the approaching and receding parts of the ring are about $-120$ to $-140$ $\mathrm{km\,s^{-1}}$ and 140 $\mathrm{km\,s^{-1}}$, respectively. The rotation is in the same direction as the rotation of the Galaxy. The radio con-

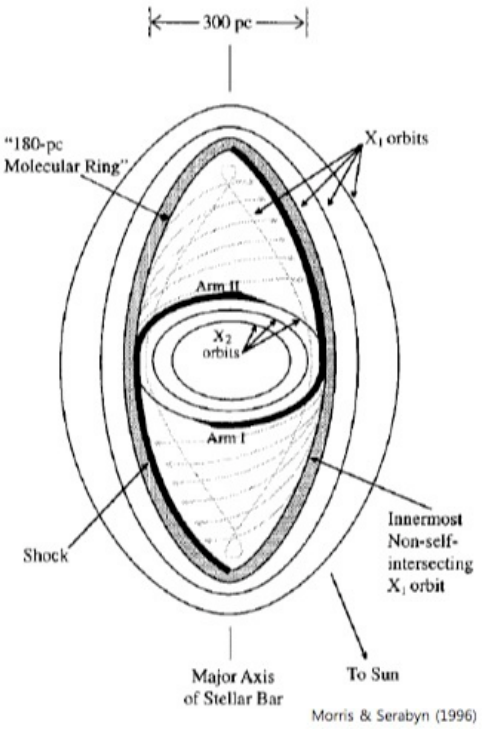


**Figure 2.8:** Stable orbits of the bar potential in the Galaxy. The 180 pc ring corresponds to the expanding molecular ring discussed in Sect. 2.1.6. (Figure by Morris & Serabyn (1996), reprinted by permission of the ARA&A).

tinuum emission indicates that the EMR is a mixture of molecular and ionised hydrogen gases. The mass of the shell, as estimated from CO observations is $\sim 10^7$ $M_\odot$, and its kinetic energy $\sim 2 \times 10^{54}$ ergs (Sofue (1995)).

The EMR also marks the location of the general H I to $H_2$ transition (Morris & Serabyn (1996). Inside the EMR is a component of dense molecular clouds located, with velocities typically $\leq$ 100 km s$^{-1}$. This population of molecular clouds includes the family of clouds in the Sgr A complex at the GC. Those gas clouds are observed not to follow star orbits (Binney et al. (1991)) but are transported inwards in the disk from losing angular momentum. In Papers II and III, we discuss our observations of the EMR, and in Paper III, we indicate a possible connection between the EMR at negative velocities and the south-west lobe of the CND.

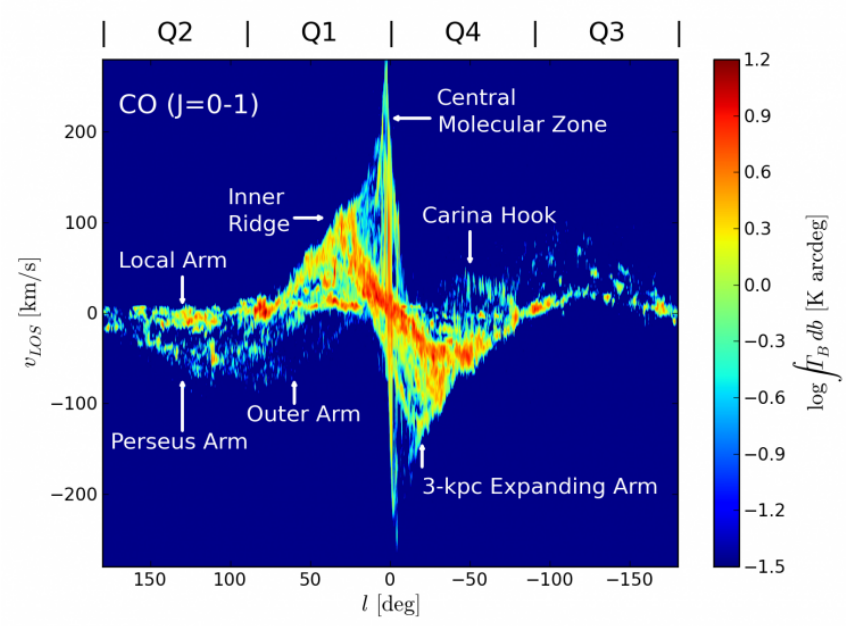


**Figure 2.9:** Galactic longitude-velocity composite image of CO $J = 1 - 0$ emission of the Galaxy derived from Dame et al. (2001) (reprinted by permission of the AAS), with labels added to selected features, amongst them the CMZ. The 3-kpc arm essentially delineates the central bar of the Galaxy.

## 2.2 The Galactic centre

### 2.2.1 General

The Galactic centre is due to its proximity the most suitable galactic nucleus for studies of kinematics, chemistry and radiation environments in an active nucleus of a spiral galaxy. Excellent reviews of the Galactic centre can be found in Brown & Liszt (1984); Genzel et al. (1994); Morris & Serabyn (1996); Mezger et al. (1996), and more recently by Ferrière (2012).

The central parts of the Galaxy cannot be observed by optical means since it is heavily obscured by thick gas and dust. Observations at other wavelengths such as $\gamma$-ray, X-ray, infrared and radio are, however, usable means to gain insight into the central parts. Much more emission than absorption data exist for the innermost regions of the GC, where gas and dust often appear to be co-located.

Molecular and ionised gas clouds are common in the disk and at the cen-

tre of the Galaxy. The molecular clouds in the Galactic centre have distinctly different physical parameters than those residing in the disk, and densities are higher, and dynamically forbidden high-velocity dispersions are observed in molecular clouds close to the Galactic centre. Gravitational instabilities and clumpiness prevail in those clouds. Magnetic fields in the innermost regions are strong (up to $\sim 2$ mG) compared with the Galactic disk, where magnetic fields of a few tens of $\mu$G are observed. The field lines are generally oriented parallel to the Galactic plane inside of giant molecular clouds and perpendicular to the plane in the intercloud medium (Mezger et al. (1996)). Within 100 pc from the centre, the magnetic field is poloidal (Morris & Yusef-Zadeh (1985)), and assumed to be responsible for the confinement of gas in the Radio arc, the Arched filaments and the threads (G0.08+0.15) in Fig. 2.7.

The inner 50 pc are populated by large amounts of gas, dust and a very high density of stars. The gas and dust are in the form of clouds of varying dimensions, and with motions of highly supersonic velocities. The velocity width of molecular clouds is greater near the Galactic centre than in the disk (Bally (1989)). The star formation rate is high in this part of the Galaxy, and the central parts also contain magnetic fields. Killeen et al. (1992) have measured magnetic field strengths in the neutral gas by Zeeman measurements of the Galactic centre of the order of 1 – 3 mG. Morris & Serabyn (1996) conclude that the magnetic fields within molecular clouds are only weakly coupled to the external magnetic fields. This result is based on an apparent immunity of observed nonthermal fields (NTF), and that molecular clouds pass through the Galactic disk without showing any appreciable large scale twist or distortion.

### 2.2.2 The Sgr A complex

Sgr A complex is a common name of the most prominent radio sources at the GC, and is located in the Sgr constellation of the sky, optically hidden behind large clouds of cosmic dust and gas. The atomic and molecular clouds in the Sgr A complex are responsible for the extinction of near-infrared emission from stars in the Nuclear bulge (Philipp et al. (1999)), which indicates that the Sgr A complex is located inside of the disk-like inner bulge (Zylka et al. (1999)). If those clouds were located behind the Nuclear bulge, there would not be extinction of the stars.

The Sgr A complex has four main continuum radio components, the halo, Sgr A East, the minispiral structure Sgr A West, and the compact radio source at the centre of the Galaxy – Sgr A*. The inner few pc at the GC contain six principal components (Melia & Falcke (2001)); the SMBH, the surrounding cluster of evolved young stars, a dusty molecular ring, ionised gas streamers, diffuse hot gas and the powerful supernova-like remnant, Sgr A East. In Her-

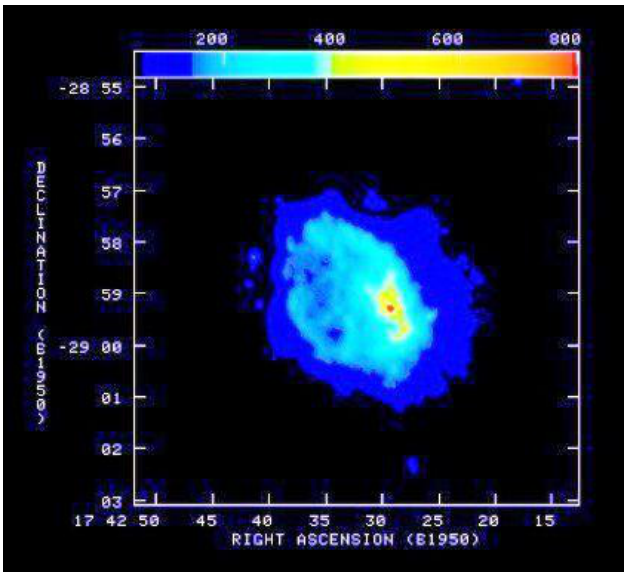


**Figure 2.10:** Sgr A complex observed at 18 cm continuum emission with the VLA, where we have concatenated the two BnA and DnC observations. The angular resolution in the image is $7'' \times 5''$, and the red spot marks the position of Sgr A*. The minispiral Sgr A West is shown in yellow, Sgr A East in light blue, and the Sgr halo in dark blue colour. The compact H II regions (Ekers et al. (1983)), are seen in dark blue east of the halo.

rnstein & Ho (2005) a cartoon is shown of the important features in the central 12 pc (Fig. 2.11), where they suggest relative positions of the objects.

### 2.2.3 Sgr A East

The nonthermal radio source Sgr A East surrounds the minispiral Sgr A West in projection, and the bubble-like shape of Sgr A East is frequently suggested as being an SNR. It has an elliptical shell structure, elongated along the Galactic plane, with a major axis of about 10.5 pc and its centre displaced from the dynamical centre by 2.5 pc towards negative Galactic latitudes. Sgr A East appears to be surrounded by a 20 pc halo, as seen in Fig. 2.12. The X-ray classification suggests that Sgr A East is a young metal-rich mixed-morphology SNR (Maeda et al. (2002)) and is the result of an event about $\sim 10^4$ years ago, pushing the surrounding material radially outwards at a velocity of about 100 $\mathrm{km\,s^{-1}}$. However, this scenario does not support the hypothesis that the four compact H II regions at the eastern edge of Sgr A East were triggered by the

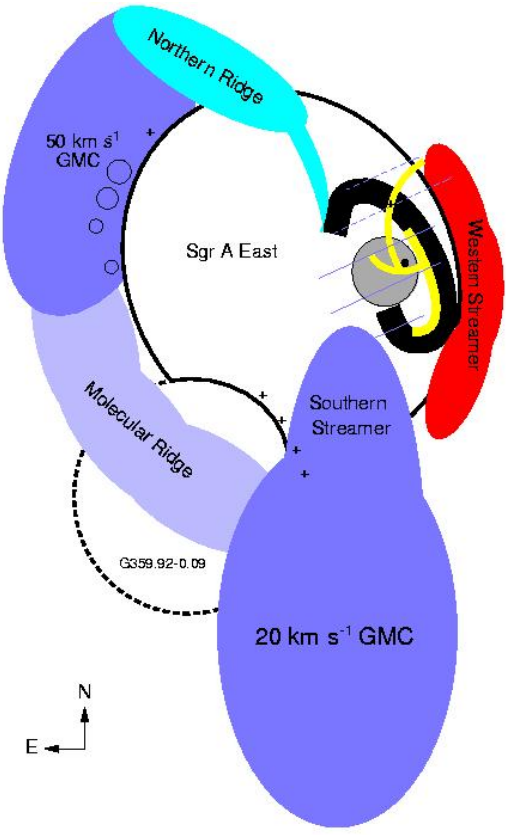


**Figure 2.11:** Cartoon of the central 12 pc of the Galaxy (Herrnstein & Ho (2005)). The CND is delineated in a thick black contour, Sgr A West in yellow and Sgr A* is the black dot inside of the star cluster shown in grey colour (Reprinted by permission of the AAS).

expanding shell, since they are considered $\sim 10^5$ – $10^6$ years old. In Karlsson et al. (2015) (Paper III), we find that all four of those compact H II regions are at least partly inside of the +50 km s$^{-1}$ cloud that arguably is compressed by the Sgr A East shell ploughing in from the west. This would imply either that the Sgr A East is, at least, a factor of 10 older, or that the compact H II regions are younger than anticipated, or are triggered by local phenomena.

Another scenario for the formation of Sgr A East was presented by Khokhlov & Melia (1996). They suggest that Sgr A East is a result of tidal disruption of a solar mass star by a $10^6$ M$_\odot$ black hole at a pericentric distance $R_\mathrm{p} \approx 10$ R$_\odot$, where R$_\odot$ is the radius of the Sun. This would result in an explosion energy of $\sim 4 \times 10^{52}$ ergs.

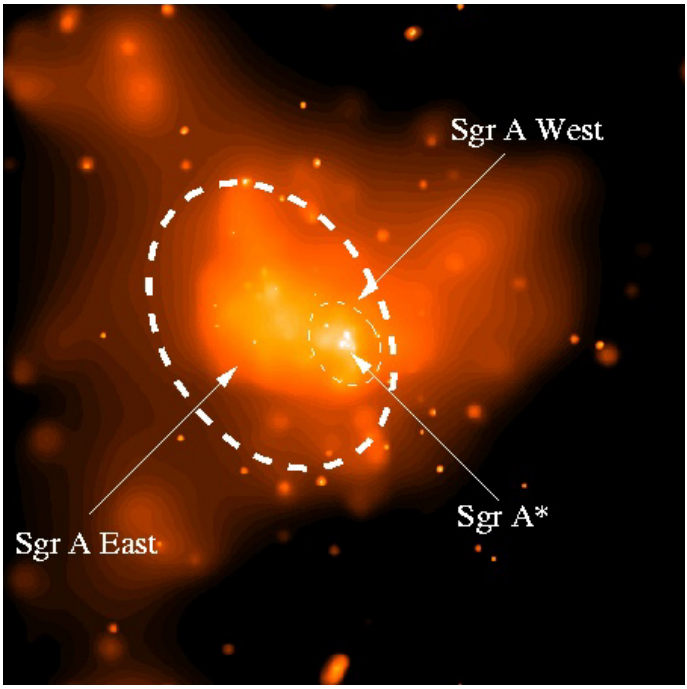


**Figure 2.12:** This Chandra X-ray image shows the relationship between Sgr A* and the supernova remnant Sgr A East. The emission from the supernova remnant Sgr A East is depicted by the bright yellow and orange colurs and its halo in faint orange shade. The dashed ellipse marks the outer edge of Sgr A East (Credit: NASA/Penn State/G.Garmire et al.).

### 2.2.4 The circumnuclear disk

The CND, Fig. 2.13, was discovered in dust emission by the Kuiper Airborne Observatory (Becklin et al. (1982)) and in HCN emission by Güsten et al. (1987), and has been the subject of many studies since then, e.g. Davidson et al. (1992) and Latvakoski et al. (1999). The CND is observed at infrared and radio wavelengths in emission and absorption in many species, e.g. $HCO^+$ Sandqvist et al. (1985); HCN Jackson et al. (1993); HCO and $HCO^+$ Christopher et al. (2005); $H_2$ Gatley et al. (1986) and Yusef-Zadeh et al. (2001); CO Liszt et al. (1985); OH Sandqvist (1974); Winnberg et al. (1985) and Karlsson et al. (2003); (2013) and (2015). A comprehensive list of observations of the CND can be found in Amo-Baladron et al. (2011). See also [1], where Morris concludes that the nature and role of the CND are crucial for understanding the complexity of the GC.

[1] *https://www.sofia.usra.edu/Science/science_cases/morris.pdf*

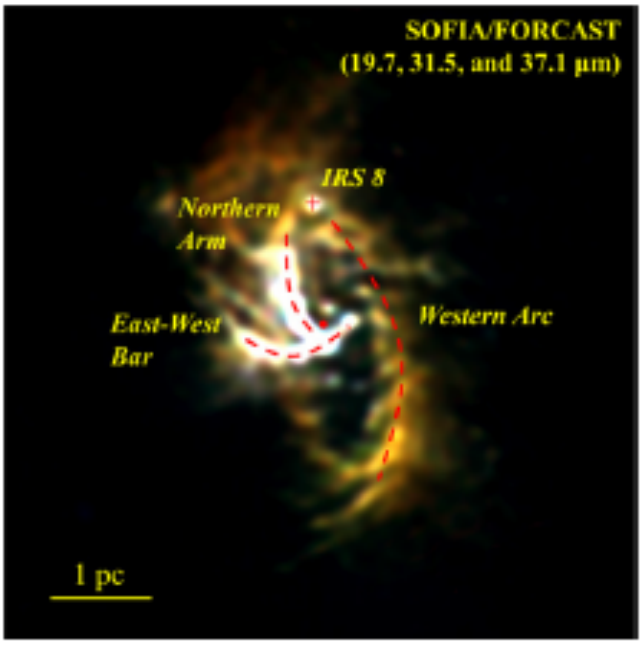


**Figure 2.13:** Composite image of the CND region in yellow shades. The dotted lines indicate Sgr A West, with the ionised streamers marked by dashed lines. The red dot is the location of Sgr A*. The deconvolved beamsize is 2".5 (Lau et al. (2013)), reprinted by permission of the AAS).

Observations of the CND reveal that it is a non-equilibrium warped ring-like structure orbiting the SMBH with a bulk rotational velocity of about 110 $\mathrm{km\,s^{-1}}$, in the same direction as the Galaxy (Güsten et al. (1987); Liszt et al. (1985) and Marr et al. (1993)). The rotation of the CND is basically Keplerian, at least in the inner parts, but it also shows noncircular motions (Jackson et al. (1993)), which are indicative of infall or outflow activities. The southwestern part of the CND is approaching us, and the northeastern lobe is receding. Outside the ring, on the west side, there is strong kinematic activity at the edge of the SW streamer matching the velocities of material in the ionised streamers (Fig. 2.13), where probably shock or tidal stripping is happening (White (1996)). The CND extends radially from about 1 to 5 pc, and the thickness is from 0.5 pc in the inner parts to about 2 pc at a radius of 5 pc. The inclination of the anticipated disk from the line of sight is about 20° – 30°, with the major axis approximately aligned with the Galactic plane, and a position angle $\sim 30°$ east of north (Güsten et al. (1987) and Jackson et al.

(1993)).

The structure of the CND is clumpy, and the velocities of clumps may locally differ from the bulk rotation velocity. Molecular and atomic gas and dust coexist in the CND. The gas temperature is generally higher than the dust temperature. The number density in the clumps is on the average $10^5$ cm$^{-3}$ (McGary et al. (2001)) but may be as high as $10^8$ cm$^{-3}$ (Christopher et al. (2005) and Jackson et al. (1993)). Line emissions at the inner part of the ring are consistent with a dense photodissociation region (PDR) as proposed by Genzel et al. (1995).

Yusef-Zadeh et al. (1996) observed an OH-maser at 1720 MHZ at 132 km s$^{-1}$ at the inner edge of the CND in the northeastern region of the CND. Karlsson et al. (2003) (Paper I) observed another 1720 MHz maser with a velocity of $-132$ km s$^{-1}$ in the southwestern part of the CND positioned opposite to the 132 km s$^{-1}$ maser. This enabled Karlsson et al. (2003), to estimate the enclosed mass inside the radius of the two opposite maser sources.

The CND is a large reservoir of mostly molecular material, and the inner parts of the CND may weakly connect to the gravitational domain of the SMBH. The CND is losing material radially inwards, probably via Sgr A West, and streams of gas, e.g. the OH-streamer, and is likely to be replenished from outside of the CND if it is a non-transient feature (Genzel & Poglitsch (1995); Coil & Ho (1999) and Karlsson et al. (2015) (Paper III)). Consequently, the CND seems to be able to fuel episodes of enhanced activities in the Galactic centre, and probably also be engaged in star formation in the central parsecs by clump-clump collisions and shock activities.

The 1 pc cavity inside of the CND is largely void of gas and dust. However, a few streamers, such as the Northern streamer and the OH-streamer, may have enough inertia to survive inward travel and sustain the strong UV-radiation in the centre region, such that material may ultimately accrete onto anticipated accretion disks or rings near the central object.

The rotation velocity of the CND indicates a rotation period of the order of $10^5$ years, and an age of $\gg 10^4$ years. However, a simple rotation model is probably oversimplifying the nature of the CND as the material in the CND is distributed highly asymmetrically about the centre. Morris & Serabyn (1996), note that asymmetry would imply a time dependence and hence a short-lived disk. There is evidence of an axisymmetric magnetic field in the CND (Hildebrand et al. (1993)). However, Novak et al. (2000) find that the magnetic field lines in the CND region are roughly directed in the north-south direction, similar to the +20 km s$^{-1}$ cloud.

The heating of the CND is subject for discussions. The total UV luminosity within the CND is $\sim 10^7$ L$_\odot$. Davidson et al. (1992) and Telesco et al. (1996), suggest that the CND is heated approximately equally by the central stellar

cluster of old stars and by the UV flux from the bright young stars clustered around the SMBH. However, Rodríguez-Fernandez et al. (2004) consider this unlikely, as it would dissociate the gas inside the radius of the ring, which is not observed. Cosmic rays are also excluded as it would heat the gas uniformly while the GMCs at the GC have a wide range of temperatures (Hüttemeister et al. (1993)), such that this group suggests cloud-cloud collisions likely to heat the neutral molecular clouds at the GC. X-ray heating is found insufficient by a factor of 3 to heat the gas (Rodríguez-Fernandez et al. (2004)). Obviously, the heating of the CND is one of many remaining questions about the CND.

Gas flows along filaments from the CND and pointing in projection to the nucleus are observed, e.g. in the Northern arm, by Davidson et al. (1992), Jackson et al. (1993), Telesco et al. (1996), and in the OH-streamer suggested by Karlsson et al. (2003) (Paper I); (2013) (Paper II) and (2015) (Paper III).

The CND itself seems to be fueled by a large molecular cloud outside of the CND, the +20 $\mathrm{km\,s^{-1}}$ cloud and the Southern streamer (Coil & Ho (1999); Okumura et al. (1991) and Karlsson et al. (2015)). The molecular belt (MB) connects the +20 and +50 $\mathrm{km\,s^{-1}}$ clouds, such that the +50 $\mathrm{km\,s^{-1}}$ cloud also could feed the CND via the +20 $\mathrm{km\,s^{-1}}$ cloud. The Northern ridge (Fig 2.11), is another candidate for the feeding of the CND (e.g. McGary et al. (2001)).

The CND is probably close to Sgr A East, see Fig. 2.11. According to Maeda & et al. (2002) and Rockefeller et al. (2005), a shock wave from Sgr A East may have distorted the morphology of the CND, and they find that the age of Sgr A East is less than 2000 years, based on X-ray observations with the *Chandra* orbital observatory.

Another scenario for the formation of the CND is suggested by Vollmer & Duschl (2002), where they suggest that the CND has resulted from the accumulation of gas from bulge stars migrating inwards in the disk. By modelling, they also suggest a scenario where the compact H II sources were formed by an encounter of a cloud $\sim$7 M years ago.

Bradford et al. (2005) combine the observations of CO $J = 7-6$ rotational transition with other CO measurements to model the physical conditions in the CND, and find that the molecular gas in this region is both warm and dense, with $T \sim 200$ – 300 K, and $n_{\mathrm{H_2}} \sim (5-7) \times 10^4$ $\mathrm{cm^{-3}}$. Moreover, Tanaka et al. (2011) find kinetic temperatures of 45 – 450 K in the CND.

The mass of warm molecular gas in the central 2 pc is at least 2000 $\mathrm{M_\odot}$, about 20 times more than the UV-excited atomic gas mass, which also rules out a UV heating scenario for the molecular material. Bradford et al. (2005) find support for a scenario in which the features near Sgr A*, such as the CND and the Northern arm, are generated by infalling clouds with low specific angular momentum. Güsten et al. (1987) and Jackson et al. (1993) estimate the infall mass rate from the CND and the material in the central cavity to be $10^{-3}$ to

$10^{-2}$ $M_\odot$ year$^{-1}$and $3 \times 10^{-2}$ $M_\odot$ year$^{-1}$, respectively.

Inside of the large clouds in the CND smaller clouds or holes are observed. The most prominent of holes is a bubble observed about 3 arcsecs southwest of Sgr A*, with an inner radius of about 1 arcsec, and known as the Minicavity. Melia et al. (1996) argue that the Minicavity is the result of impact by a bow-shock in gas flowing out from Sgr A* at $500 - 700$ km s$^{-1}$, while Roberts et al. (1996), hypothesised that it is an ionised part of a molecular cloud in hyperbolic orbit about Sgr A*.

Recently, Lau et al. (2013), observed the CND region in dust emission with the Stratospheric Observatory for Infrared Astronomy (SOFIA) with the Faint Object Infrared Camera (FORCAST), with an angular resolution of $3''.2$ – $4''.6$. They found a clumpy ring, circumnuclear ring (CNR), of dust located inside of the CND. The dust emission resembles the ionised gas and photodissociation regions. The dust temperatures were found to be between 65 and 85 K, indicating that the dust is heated by the hot young stars inside of the CNR. The clumps inside of the CNR were found to be transient objects with a lifetime of about $10^5$ years, i.e. about one orbital period of the CND. In Fig. 2.14 their modelling of the CNR is presented.

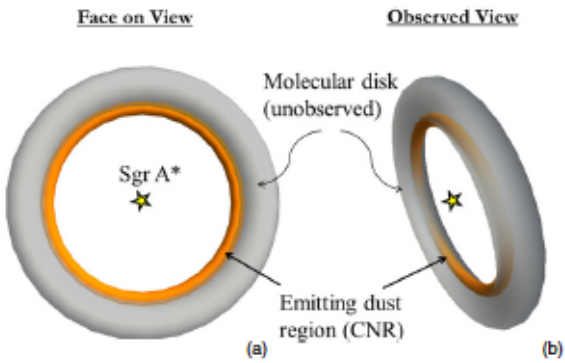


**Figure 2.14:** Schematic sketch of the CNR. The inner (orange) ring is the illuminated inner ring, while the outer (grey) ring is cool gas and dust. The north and south regions of the CNR in the right panel are enhanced to emphasize the higher column density of the emitting dust (Lau et al. (2013), reprinted by permission of the AAS).

### 2.2.5 Sgr A West

Sgr A West appears projected on the sky as a three-arm spiral object, consisting of the Northern and Eastern arms, the Western arc, and a bar-like region called the Bar. The western part of Sgr A West coincides in projected position with the inner ionised edge of the CND. Sgr A West is often referred to as the "minispiral". The apparent spiral features are a collection of arcs in the cavity of the CND where gas is observed to travel (Paumard et al. (2004)). Some of the arcs appear to feed material into the nucleus (Lo & Claussen (1983); Roberts & Goss (1983) and Zhao et al. (2009)). The origin of the minispiral is likely to be instabilities in the CND or collisions of molecular clouds with portions of the CND (Morris & Serabyn (1996), and references therein). The surface layers of Sgr A West are ionised, and the source of ionisation is considered to be UV-radiation from a population of massive stars in the central parsec of the Galaxy. The dynamics and 3D structure of the Northern arm, Eastern arm, Western arc, and the Bar region have been extensively studied by Zhao et al. (2009). They have modelled the velocity field in Sgr A West and suggest that the Eastern arm and the Bar region are not in the same plane as the Northern arm (Fig. 2.15).

Zhao et al. (2009) confirm earlier results that motions in the Western arc and the Northern arm are in Keplerian motion and that the Eastern arm is in an elliptical orbit, all in a counterclockwise motion around Sgr A*, with orbital periods of $(4-8)\times 10^4$ years. The Northern and Eastern arms have large eccentricities while the Western arc is in a nearly circular motion. The computed orbits (Fig. 2.15, right panel), suggest that the streams in the Northern and Eastern arms collide in the Bar region and that most of the orbiting gas is behind Sgr A*. Zhao et al. (2009) also note the helical structure of the Northern arm is indicative of MHD influence on the ionised gas. The Northern arm seems to be a stream of gas responsible for the feeding of material from outside molecular clouds into the SMBH at the centre. Furthermore, a linear feature in the IRS 16 region, which is a cluster of some twenty bright stars a few arcsecs east of Sgr A*, suggests that the compressed edge of the Northern arm results from collective winds and radiation pressure from the high mass IRS 16 cluster.

Towards the Minicavity, a large velocity gradient ($> 600$ km s$^{-1}$ pc $^{-1}$) is observed along the eastern rim and uniformly large velocities are observed along the western rim of the Minicavity. The velocity field of the Minicavity is interpreted as gas in a hyperbolic orbit about Sgr A* (Gillessen et al. (2009)).

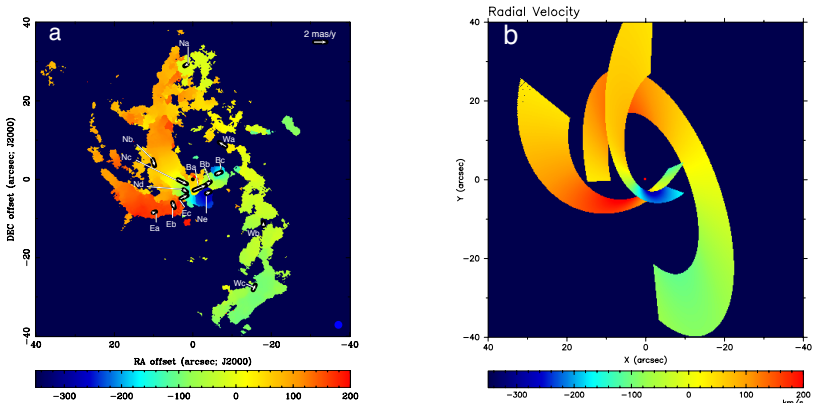


**Figure 2.15:** Comparison of observed (left panel) and a numerically calculated model (right panel) of Sgr A West. The radial velocities are displayed in colour, and the transverse velocities (very small white vectors in the left panel), are determined from proper motions (Zhao et al. (2009), reprinted by permission of the AAS).

### 2.2.6 The molecular belt

The molecular belt (MB), or molecular ridge, is observed in both emission and absorption and connects the +50 km s$^{-1}$ molecular cloud in the northeast with the +20 km s$^{-1}$ cloud south of Sgr A* (e.g. Karlsson et al. (2013), Paper II). In Fig. 2.16, the MB is seen in dust emission on an overlay of a 2.2 $\mu$m image. See also the stretch of the MB modelled in Fig. 2.11. There is a gradient of decreasing velocities from the +50 km s$^{-1}$ cloud to the +20 km s$^{-1}$ cloud (e.g. Sandqvist (1989) and Karlsson et al. (2013)). The +50 and +20 km s$^{-1}$ clouds and the MB are located in the central 10 – 30 pc of the Galactic centre and interact with Sgr A East (e.g. Ho et al. (1985); Pedlar et al. (1989); Zylka et al. (1990); Genzel et al. (1990), and Okumura et al. (1991)).

The mass of the two GMCs, the +50 and +20 km s$^{-1}$ clouds, are a few $10^5$ $M_\odot$ and $n_{H_2} \sim 10^4$ – $10^6$ cm$^{-3}$. The gas temperature is $\geq$ 40 K, but the dust temperature is only about 20 K (Mezger et al. (1989); Zylka et al. (1990) and Genzel et al. (1990)). The MB and its relation to the +20 and +50 km s$^{-1}$ clouds are discussed in Papers I, II and III, Karlsson et al. (2003); (2013) and (2015), respectively.

### 2.2.7 The +50 km s$^{-1}$ molecular cloud

The +50 km s$^{-1}$ cloud (Güsten et al. (1981)) is a GMC, observed in many species, e.g. in OH absorption, C$^{18}$O, CS and $NH_3$ emissions. It is projected

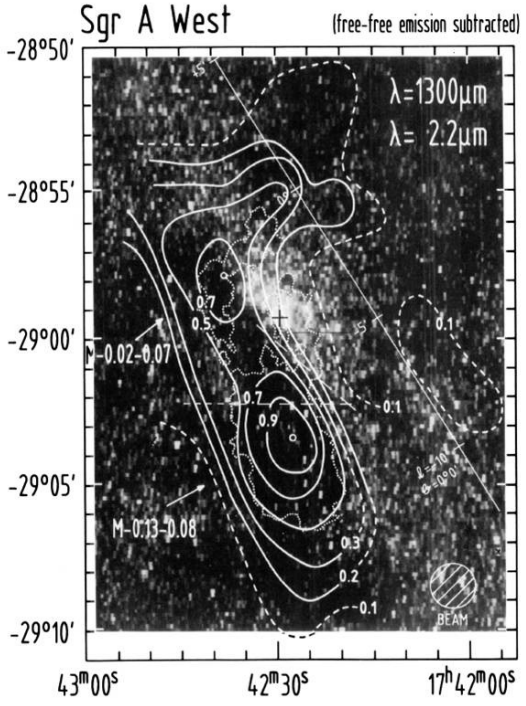


**Figure 2.16:** Dust emission at 1.3 mm (contours) overlaid on a 2.2$\mu$m image by Glass et al. (1987). The MB is seen as stretching from the +50 km s$^{-1}$ cloud in south-westerly direction to the +20 km s$^{-1}$ cloud (Zylka et al. (1990), reproduced with permission ©ESO).

on the eastern edge of the expanding Sgr A East shell and wraps around both the near and far side of the shell. In the OH 1667 MHz $-T_{\rm L}/T_{\rm C}$ apparent opacity maps (Fig. 2.18), the +50 km s$^{-1}$ cloud is seen in OH at velocities between 24 and 76 km s$^{-1}$. The western side of the cloud is concave which indicates that the Sgr A East shell is ploughing into the +50 km s$^{-1}$ cloud. Several 1720 MHz OH masers are observed along the western edge, possibly as a result of the compression of the gas by the expanding shell. 1720 MHz masers are also observed in the region of the compact H II regions. The south-east side of the +50 km s$^{-1}$ cloud may also interact with the MB (Karlsson et al. (2003) and (2013), Papers I and II). The mass of the +50 km s$^{-1}$ cloud is of the order of a few $10^5$ M$_\odot$ (Ferrière (2012)).

On the eastern edge of the +50 km s$^{-1}$ cloud, the four compact H II regions A-D (Ekers et al. (1983)), are observed. In Karlsson et al. (2015) (Paper III), we find that all four of the compact H II regions are at least partly embedded in

the +50 $\mathrm{km\,s^{-1}}$ cloud. In Paper II, we suggest that the star-forming processes in those regions may have been triggered by local shock fronts seen in our $C^{18}O$ observations.

### 2.2.8 The +20 $\mathrm{km\,s^{-1}}$ molecular cloud

The +20 $\mathrm{km\,s^{-1}}$ cloud (Güsten & Downes (1980)) is located south of Sgr A* in a north to south direction seen at a velocity of 32 $\mathrm{km\,s^{-1}}$ in Fig. 2.17 and between 15 and 32 $\mathrm{km\,s^{-1}}$ in the apparent opacity map of Fig. 2.18. Its projected dimensions are $\sim$ 15 pc $\times$7.5 pc (Ferrière (2012)). The +20 $\mathrm{km\,s^{-1}}$ cloud is generally observed in the same species as the +50 $\mathrm{km\,s^{-1}}$ cloud. The northern tip of the +20 $\mathrm{km\,s^{-1}}$ cloud is called the Southern streamer, and is arguedly feeding the CND south-western lobe (e.g. Ho et al. (1991)). The mass of the +20 $\mathrm{km\,s^{-1}}$ cloud is of the order of $2\times\ 10^5$ $\mathrm{M_\odot}$ (Ferrière (2012)). A discussion of the +20 $\mathrm{km\,s^{-1}}$ cloud and its interactions is given in Karlsson et al. (2013) and Karlsson et al. (2015) (Papers II and III).

### 2.2.9 The OH-streamer

The OH-streamer was detected in absorption in the 1612, 1665 and 1667 MHz transitions of OH (Sandqvist et al. (1987); Karlsson et al. (2003) Paper I and (2015) Paper III). In projection, it runs from the inner parts of the CND SW lobe towards the GC, between velocities of $-29$ and 67 $\mathrm{km\,s^{-1}}$ (Fig. 2.17). It has three main parts, the Head, Mid and Tail. A clumpy structure is seen inside of the Mid part (Fig. 2.17). The Tail is about 1.5 pc from Sgr A*, and the Head seems to embed the GC at a radius of about 0.2 pc, projected distances, respectively. The full stretch of the OH-streamer is not seen in other species. However, parts of the Head are observed in CN $J = 2-1$ emission (Martín et al. (2012)), and blobs of CN emission and weak radio emission are observed at spatial positions adjacent to some of the clumps in the OH-streamer Mid part (Yusef-Zadeh et al. (2012)). Killeen et al. (1992) also detected the OH-streamer in OH absorption at 1667 MHz in their investigation of magnetic fields at the GC. They did, however, not find magnetic fields at the 3 $\sigma$ level ($1-3$ mG) in the OH-streamer. In Fig. 2.19, the OH-streamer, the +80 $\mathrm{km\,s^{-1}}$ cloud and the CND SW lobe, are overlaid. The positional coherence is intriguing. However, the velocities between the OH-streamer and the CND SW lobe differ by more than 100 $\mathrm{km\,s^{-1}}$ at 1667 MHz at positions that coincide in the map plane.

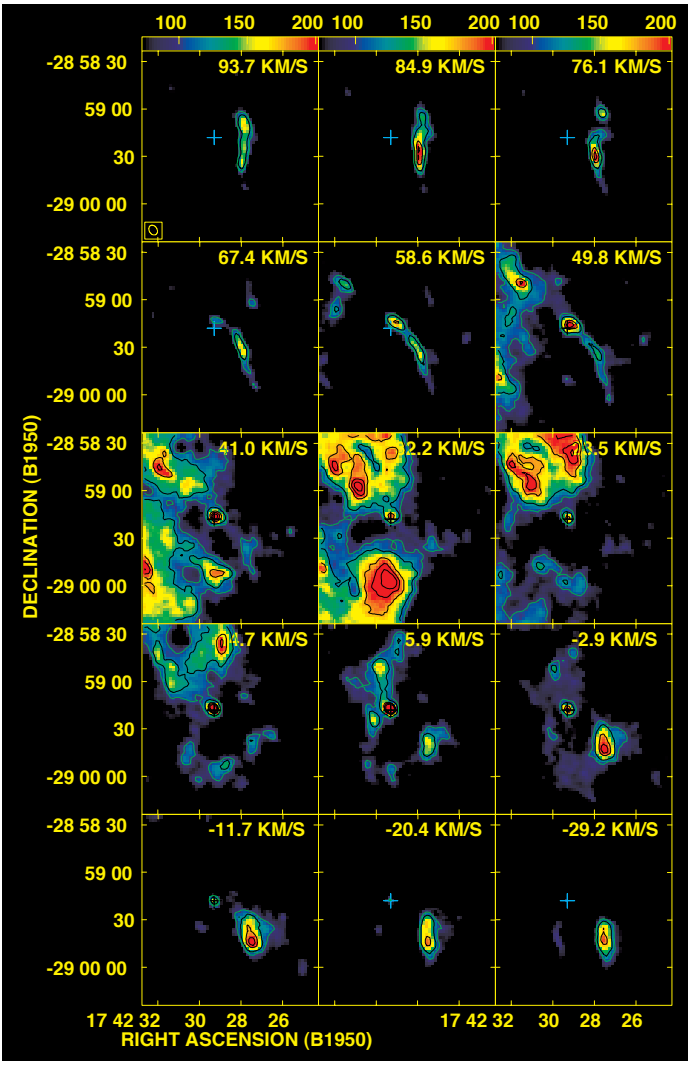


**Figure 2.17:** OH absorption against the inner 4.4 pc of the GC at 1667 MHz, at velocities between $-29$ and 94 $\mathrm{km\,s^{-1}}$. Sgr A* is marked by a plus sign. The +80 $\mathrm{km\,s^{-1}}$ cloud is seen at velocities from 76 to 94 $\mathrm{km\,s^{-1}}$, the OH-streamer between $-29$ and 67 $\mathrm{km\,s^{-1}}$, the SS and the +20 $\mathrm{km\,s^{-1}}$ cloud are seen between $-32$ and 41 $\mathrm{km\,s^{-1}}$, south of Sgr A*. The lowest contour level is $\sim 3\sigma$, and the contour spacing is $\sim 1\sigma$. The wedge scale is in mJy/beam, and the beam size is shown in the lower left corner of the uppermost left panel in the figure (Paper III, Karlsson et al. (2015), reproduced with permission ©ESO).

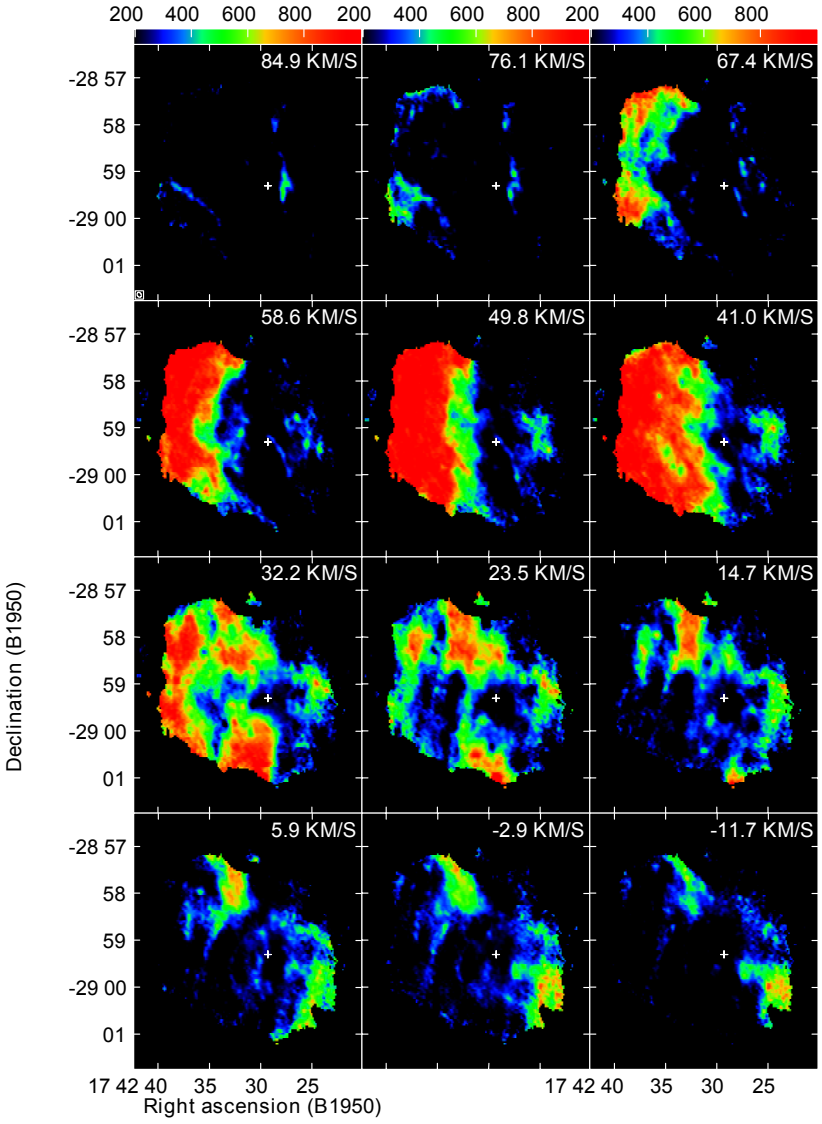


**Figure 2.18:** $-T_{\rm L}/T_{\rm C}$ OH apparent opacity distribution at 1667 MHz. The +50 km s$^{-1}$ cloud is seen E of Sgr A* at velocities between 24 and 76 km s$^{-1}$, the SS and the +20 km s$^{-1}$ cloud are located S of Sgr A* at velocities between 15 and 32 km s$^{-1}$, and the +80 km s$^{-1}$ cloud appears W of Sgr A* at 67 to 85 km s$^{-1}$. The OH-streamer is seen at velocities between 41 and 67 km s$^{-1}$. The position of Sgr A* is marked with a plus sign. The wedge scale is the ratio multiplied by 1000, the angular resolution in the map is 7"$\times$ 5", and the beam size is shown in the lower left corner of the uppermost left panel in the figure (Paper III, Karlsson et al. (2015), reproduced with permission ©ESO).

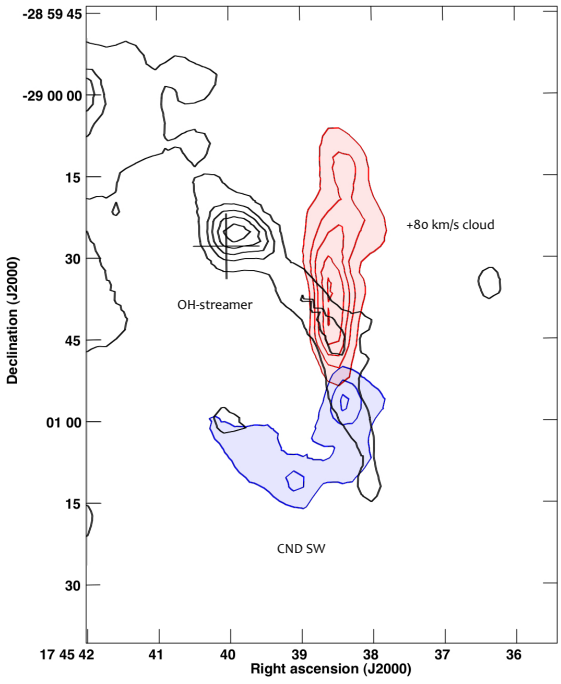


**Figure 2.19:** OH absorption at 1667 MHz of the OH-streamer at 50 $\mathrm{km\,s^{-1}}$ with overlays of the +80 $\mathrm{km\,s^{-1}}$ cloud at 85 $\mathrm{km\,s^{-1}}$, and the SW lobe of the CND at $-73$ $\mathrm{km\,s^{-1}}$. The lowest contour level is drawn at $\sim 90$ mJy/beam ($\sim 3.5\sigma$) and the contour spacing is $1\sigma$. Sgr A* is marked with a plus sign (Karlsson et al. (2015), reproduced with permission ©ESO).

### 2.2.10 The +80 $\mathrm{km\,s^{-1}}$ cloud

The +80 $\mathrm{km\,s^{-1}}$ cloud was first detected in HCN emission and referred to as the "redshifted cloud" by Güsten, et al. (1987), and they concluded that the relationship of this redshifted cloud to the CND was not well understood. The same cloud was observed in 18 cm OH absorption by Sandqvist et al. (1987) and referred to as "another feature at +78 $\mathrm{km\,s^{-1}}$". In Fig. 2.17 the +80 $\mathrm{km\,s^{-1}}$ cloud is seen as a nearly vertical structure west of Sgr A*, between velocities of 76 and 94 $\mathrm{km\,s^{-1}}$. Killeen et al. (1992), also observed the cloud in OH absorption at 1667-MHz. Jackson et al. (1993) and Marshall et al. (1995) note that the "+70 $\mathrm{km\,s^{-1}}$ feature" is unrelated to the ring of clouds (i.e. the CND), but instead is a separate cloud in the position-angle vs. velocity diagram (Fig. 2.20). The same conclusion can be drawn from Fig. 9 in Martín, et al. (2012). However, Karlsson et al. (2015) (Paper III) suggest a relation between the

CND, the OH-streamer and the +80 $\mathrm{km\,s^{-1}}$ cloud.

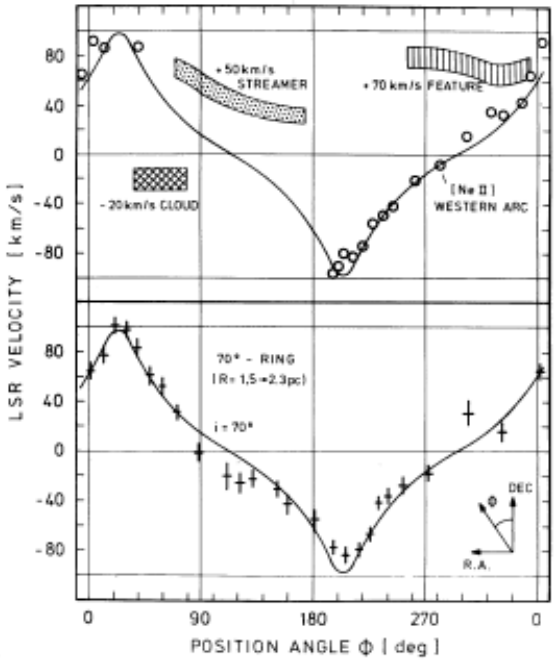


**Figure 2.20:** Velocity centroids of selected molecular gas features at $1.5 - 2$ pc from the GC. The theoretical curve for a rotating ring with a rotation velocity of 100 $\mathrm{km\,s^{-1}}$, is drawn. Open circles represent velocities in the western arc from Ne II observations by Serabyn & Lacy (1985) (Fig. 4 in Jackson et al. (1993), reprinted by permission of the AAS).

### 2.2.11 The four compact H II regions on the eastern edge of Sgr A East

The four compact H II regions (A-D), are located on the eastern edge of the Sgr A East shell and were first detected by Ekers et al. (1983) in their observations with the VLA at 6 cm. Later studies of the four compact H II regions have been made by Goss et al. (1985); Serabyn et al. (1992); Yusef-Zadeh et al. (2010), and Mills et al. (2011), see Fig. 2.21.

Goss et al. (1985) observed in the H76$\alpha$ recombination line with the VLA at a resolution of 3 arcsecs, and note that the compact H II regions are regions of recent star formation and may be associated with the +50 $\mathrm{km\,s^{-1}}$ cloud. Serabyn et al. (1992) observed the Ne II and Ar III transitions and conclude

that the four compact H II regions originated from star formation prior to the epoch when the Sgr A East shell impacted the +50 km s$^{-1}$ cloud. Yusef-Zadeh et al. (2010) observed the ionised gas in the Ne II line emission, and found that the morphology of the most compact source (D) is different from the A-C sources and suggest that the emission from D emanated from mass loss from a massive young star. Mills et al. (2011) observed the hydrogen Paschen-alpha emission and also discussed mass loss via a disk or ring surrounding the source D.

Karlsson et al. (2013) (Paper II) further discuss the compact H II regions, and conclude that source D is located inside or partly inside of the +50 km s$^{-1}$ cloud and shows a bipolar molecular structure observed in C$^{18}$O emission. In Paper III (Karlsson et al. 2015), we note that a renewed evaluation of the data reveals that all four sources A-D are seen in OH-absorption, implicating that all the compact H II regions are located inside or partly inside of the +50 km s$^{-1}$ cloud.

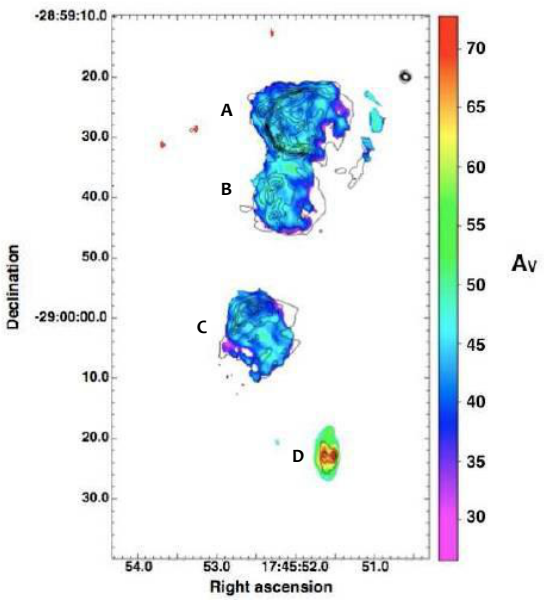


**Figure 2.21:** Observation of the four compact H II regions on the eastern edge of the Sgr A East shell observed in Paschen-alpha emission with identifying letters overlaid. The coordinates refer to J2000 (Mills et al. (2011), reprinted by permission of the AAS).

### 2.2.12 The high negative velocity gas

The high negative velocity gas (HNVG), was first discussed in the literature by Güsten & Downes (1981), who observed in H I and $H_2CO$ and ruled out rotation about the GC, and instead suggested an ejection model where the gas would flow out from the Galactic nucleus. Yusef-Zadeh et al. (1993) observed the HNVG with the VLA at velocities between $-211$ and $-160$ km s$^{-1}$. This group favoured a relation to the rotating molecular disk at the GC.

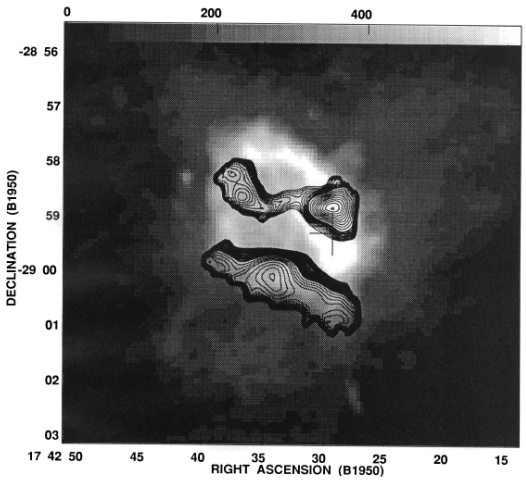


**Figure 2.22:** H I gas optical depth map showing the southern and northern lobes of the HNVG, integrated over $-206$ to $-180$ km s$^{-1}$ and $-175$ to $-160$ km s$^{-1}$, respectively (Yusef-Zadeh et al. (1993)). The grey scale is the 20 cm image of Sgr A from Yusef-Zadeh & Morris (1987) (Reprinted by permission of the AAS).

Zhao et al. (1995) observed the HNVG in H I and OH absorption and found that the observed kinematics of the gas is neither consistent with the ejection of material, nor with the expanding molecular ring. Instead Zhao et al. (1995) suggest that the HNVG is a tidally disrupted cloud that flows towards the GC, based on modelling of the cloud. In Paper I, Karlsson et al. (2003) observed a double-lobed structure of the HNVG.

### 2.2.13 Sgr A*

By using the NRAO three telescope radio interferometer at Green Bank, Balick & Brown (1974) discovered a strong point-like nonthermal broad band emission radio source ($T_B \gtrsim 10^7$ K) in the Sagittarius constellation in the direction of the Galactic centre, Sgr A*, which seemed embedded in the H II region Sgr

A West. The radio spectrum, integrated over the central pc of the GC, is complex but resembles in many respects that of a Seyfert galaxy. A Seyfert galaxy is a galaxy with an active nucleus, emitting with very high luminosity at certain portions of the electromagnetic spectrum. The luminosity of Sgr A* is, however, very dim $\sim 10^{36}$ ergs, compared to other active galaxies. Nevertheless, the Galaxy is considered as an active galaxy, but possibly in a dormant state.

Sgr A* is observed to have at least two states: a quiescent steady-state showing X-ray flux variations on a one-year time scale, and an overlaid flare state with flux variations on time scales less than one hour. A typical short time flare duration is 20 minutes to 1 hour, and the luminosity may increase by orders of magnitude during such times. The source is brightest in the millimetre radio band with a spectral distribution indicative of composite radiative processes, such as thermal bremsstrahlung and synchrotron self-Compton emission, as well as emission from young Wolf-Rayet (WR) stars.

Activities in Sgr A* are also observed on time scales as short as ten minutes, but signs of activity on hundred-year time scales or more have also been anticipated. Time variations of 100 – 1000 years were modelled by Cuadra et al. (2005). They found that accreting of gas surrounding Sgr A* would give rise to strong X-ray variability, which is consistent with observations with the *Chandra* X-ray orbiting observatory (Baganoff et al. (2003)). Other arguments are found that Sgr A* was subject to periods of increased activity lasting thousands of years and expelled a bipolar outflow perpendicular to the Galactic plane (Baganoff et al. (2003)).

The spectrum of Sgr A* is a mix of three components: an inverted centimetre wave spectrum ($< 100$ GHz), a submillimetre hump (100 – 1000 GHz), and a steep infrared cut-off at $> 10^3$ GHz. Flat radio emission spectra are characteristic signatures of jets, where radio plasma is freely expanding in a supersonic jet. The flat spectrum appearance is a superposition of self-absorbed synchrotron spectra and results from the sum of radiation at all wavelengths. The shortest observed time scale of fluctuations in the radio emission of Sgr A* ($\sim$ 10 minutes) implies a size of $\sim 20\ R_{\mathrm{s(SMBH)}}$, where $R_{\mathrm{s(SMBH)}}$ is the Schwarzschild radius of the SMBH, i.e. $\sim 0.085$ Astronomical units, or about 2000 times the radius of the Earth.

### 2.2.14 Mass of the supermassive black hole at the centre of the Galaxy

Determination of the mass of a central supermassive black hole can be made by indirect methods based on dynamics of matter outside of the SMBH. The most accurate determination of the mass of the compact object at the centre of

the Galaxy may be calculated from stellar proper motions close to the centre. Star motions directly probe the gravitational potential and are not affected by other forces such as radiation, thermal pressure or magnetic fields. Eckart & Genzel (1997) and Genzel at al. (1997), discovered a group of orbiting stars close to the SMBH, which subsequently enabled estimation of the SMBH's mass. Using the Keck telescope, Ghez et al. (1998) confirmed the existence of those orbiting stars. With the advent of the Very Large Telescope (VLT) with adaptive optics technique, star motions at tenths of arcsecs from the GC have been observed in near-infrared emission. Orbital elements of such stars have been established (Schödel et al. (2002); Genzel et al. (2003); Eisenhauer et al. (2005)). About 30 massive young massive WR stars have been observed at distances less than 0.5 pc from the GC, distributed in two disks nearly perpendicular to each other (Genzel et al. (2003)). Moreover, stars with extreme orbital velocities, hypervelocity stars (HVS), have been observed (Fig. 2.23), and show that stellar orbits are Keplerian up to a distance of about 30 light days. The stellar proper motions have revealed a dark concentration of mass at the centre of gravity that coincides with the position of Sgr A*, within 0.01 light years (Ghez et al. (1999)). Acceleration of stars in orbit around the centre have been measured by Ghez et al. (2000) and Eckart et al. (2001), which locates the centre of mass with even higher precision. Sgr A* is observed not to move relative to the GC, which is another indication of Sgr A* being the true dynamical centre of the Galaxy, and that this object is an SMBH. Meyer et al. (2012), observed a star with an even shorter orbital period, namely 11.5 years. The estimates of the mass of the SMBH varies greatly in the literature, e.g. Eisenhauer et al. (2005) estimate the mass of the SMBH to be $3.6\pm0.3 \times 10^6$ $M_\odot$, Gillessen et al. (2009) quote $4.31\pm0.06 \times 10^6$ $M_\odot$, and Chatzopoulos et al. (2014) give a value of $3.88\pm0.14\times 10^6$ $M_\odot$. In a recent review of Mapelli & Gualandris (2016) the mass of the SMBH was found to be (3.6 +0.2/-0.4) $\times 10^6$ $M_\odot$, by a best fitting of the values given in the literature. The results are, however, dependent on the assumed distance to the GC, which differ among the studies made. For our purpose here, we have used the value given by Eisenhauer et al. (2005) in Fig. 2.24.

Karlsson et al. (2003) (Paper I) assumed a distance of 8.0 kpc from the centre, and estimated the mass inside a radius of 1.84 pc, to be $7.5 \times 10^6$ $M_\odot$ including the SMBH, stars, dust and gas. Our result in Paper I of the enclosed mass agrees well with the mass estimate by Mapelli & Gualandris (2016) for a CND that rotates with 110 $\mathrm{km\,s^{-1}}$. In Fig. 2.24 we have marked our value with its error bar.

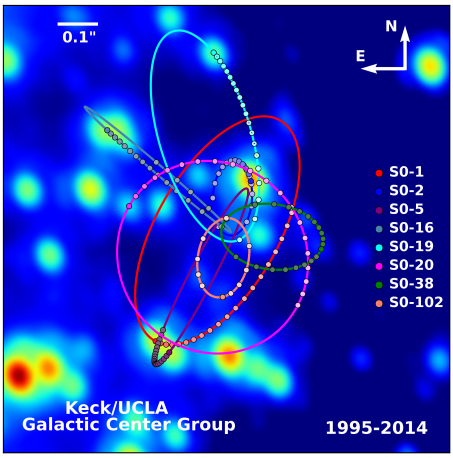


**Figure 2.23:** Orbits of stars within the central 1" × 1" of the Galaxy. Movements of every star in this image have been observed between 1995 and 2014. The annual average positions for these eight stars are plotted as colored dots. Also plotted are the best fitting simultaneous orbital solutions (Credit: UCLA Galactic Center Group - W.M. Keck Observatory Laser Team).

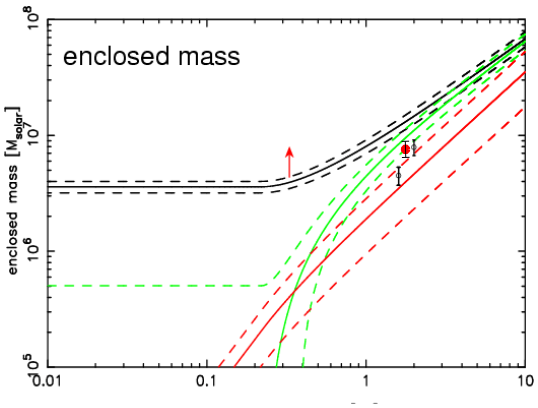


**Figure 2.24:** Estimate of enclosed mass versus projected distance from Sgr A* (black line) by Mapelli & Gualandris (2016) (Springer license number 3796430846457). The open circles at, 1.6 and 2 pc, indicate the mass estimates for assumed rotation velocities of 110 and 130 $\mathrm{km\,s^{-1}}$, respectively, for the CND. The red dot marks the mass estimate by Karlsson et al. (2003).

The OH-streamer stretches from about 2.5 pc projected distance from the GC and seems to sweep around the position of Sgr A*. To understand how the gravitational field in the vicinity of the SMBH may affect the OH-streamer we have calculated the specific gravitational force in this region.

The influence radius of the SMBH can be calculated from Sanders (1998),

$$\mathcal{F} = \frac{8.9 \times 10^2}{r^2}\left[\frac{r}{r_c} - \arctan\frac{r}{r_c}\right] + \frac{4.3 \times 10^3}{r^2} \times \frac{M_{\rm SMBH}}{10^6 M_\odot} \qquad (2.1)$$

where $r_c$ = core radius, assumed at 0.085 pc, and the mass of the SMBH = $3.7 \times 10^6$ M $_\odot$. The specific force $\mathcal{F}$ is derived in units of km$^2$/s$^2$/pc.

In Fig. 2.25, the total gravitational force is plotted against the distance from a $3.7 \times 10^6$ M$_\odot$ SMBH and a core radius of 0.085 pc. It can be seen in the figure that the total gravitational force at the OH-streamer Head (< 0.2 pc) is about two orders of magnitude stronger than at the Tail at about 1.5 pc.

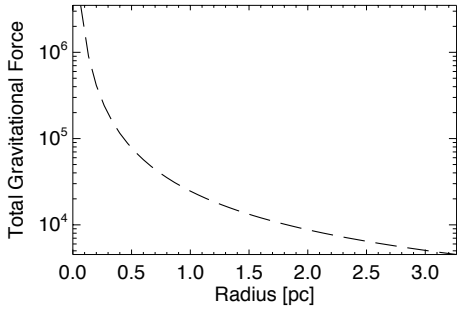


**Figure 2.25:** Range of total gravitational force (in units of km$^2$/s$^2$/pc) are plotted against the distance in pc from a $3.6 \times 10^6$ M$_\odot$ SMBH.

# 3. Observations

## 3.1 Radio astronomical observations

A basic problem of astronomical observations is to reveal the 3D geometry, i.e. the morphology in all three axes in space. By measuring the Doppler shift of frequency from a known rest frequency, the line-of-sight velocity of an object may be inferred. However, transverse motions are generally not possible to observe, unless observations of high-velocity objects can be made at different epochs. Common means to understand the 3D-structure are assumptions on geometry and fitting of models or a combination of those methods. As a first order method, absorption measurements are useful, and may give information whether objects are in front of a continuum source.

The observed image of a radio telescope does, however, not resemble the true intensity distribution, but is modified (convolved) by the beam of the telescope, such that $b' * I = I'$, where $b'$ is the beam, $I$ is the true brightness distribution, $I'$ is the observed map, and $*$ means convolution. Signal noise is another source of uncertainty since most objects are extremely faint. These problems can, however, strongly be eliminated by algorithms for beam restoration and noise reduction run on contemporary computer systems.

## 3.2 Molecular clouds

Information about atoms, molecules and dust in interstellar space came historically only from optical observations. i.e. from a very narrow band of the energy spectrum, as seen in Fig. 3.1. The utilization of radio telescopes since the 1930-s and on, has opened a new field of observations compared to a study of radiation only at visible wavelengths. A much wider window has been opened for observations because most of the energy transitions in atoms and molecules take place in the radio and infrared regimes of the spectrum. However, the much longer wavelengths of radio and infrared radiation limit the angular resolution by orders of magnitude compared with optical instruments. For example, an optical instrument placed on the Earth is limited (by the atmosphere) to an angular resolution of about $0.5''$. A 100-meter single dish radio telescope would have an angular resolution of only about $500''$ ($8'$) at a wave-

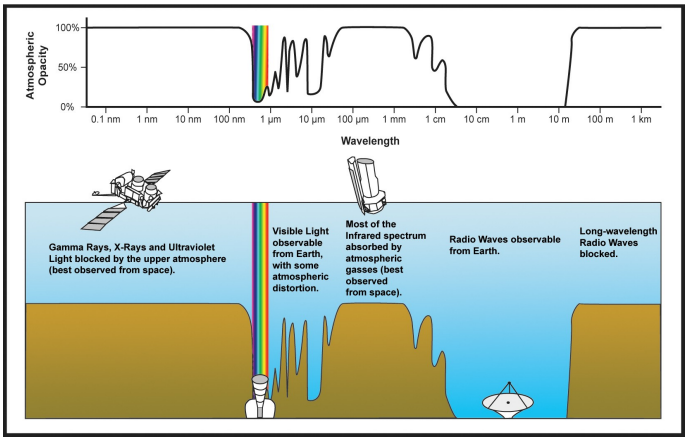


**Figure 3.1:** Transmission windows in the Earth's atmosphere (Courtesy NASA/JPL-Caltech).

length of 21 cm. Fortunately, the poor angular resolution at radio wavelengths can largely be overcome by the use of interferometers and aperture synthesis, i.e. smaller telescopes arranged in an array and connected.

Direct observation of molecular clouds is, however, restricted since the main constituent, $H_2$, is difficult to detect. Other atoms and molecules are, however, mixed with the hydrogen content and make molecular clouds observable at other wavelengths in the radio and infrared regimes of the spectrum. For example, CO is very abundant and easily observable and may be used as a proxy for $H_2$. By observing energy transitions of different species, properties of molecular clouds and their motions may be inferred. Dust and gas are often observed to move together in the interstellar space, and observations of dust at infrared wavelengths may also indicate the presence of gas.

In the line of sight towards the GC, several foreground objects are located, such as spiral arm features (Fig. 2.3), and should be taken into account in observations. In Fig. 3.2 some of those are shown with their often used designations.

## 3.3 Observational strategy

OH is abundant in molecular clouds in the Galaxy and is observed both in absorption and emission at 18 cm. In addition to the strong OH masers discovered at 1665 MHz in star formation regions, OH is also masing in the satellite transition lines of 1612 and 1720 MHz. The 1612 MHz masers can be used for tracing radiative pumping in circumstellar shells in OH/IR-sources while 1720

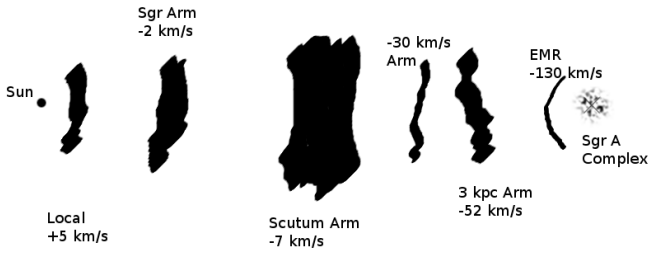


**Figure 3.2:** Line of sight features towards the GC (Sandqvist et al. (2015), reproduced with permission ©ESO).

MHz maser activity is indicative of collisional pumping processes at shock fronts. Moreover, observation of the OH main transition lines in absorption is a proper tool for revealing locations of objects relative to a continuum source, and the relative intensities of the 1665 and 1667 MHz lines may be used to infer on opacities in OH molecular clouds.

Before the advent of astronomical radio interferometers, lunar occultation methods were used for obtaining high-resolution information about OH in the GC. For example, Sandqvist (1970); (1973) and (1974) published OH absorption line investigations based on observations of the lunar occultations in 1968-1970, made with the 140-feet radio telescope at Green Bank, operated by the National Radio Astronomy Observatory (NRAO). The angular resolution of about 40 arcseconds was just enough to resolve some of the discrete features at the GC.

In 1974, Whiteoak and Gardner, at the Commonwealth Scientific and Industrial Research Organisation (CSIRO), in Epping Australia, observed OH spectral line transitions at 1612 and 1720 MHz with the 64 m Parkes single dish telescope. The beamwidth was $12'$ at 18 cm (Whiteoak & Gardner (1975) and (1976)). Among other things, Whiteoak & Gardner detected a narrow emission feature in the 1720 MHz transition at 132 $\mathrm{km\,s^{-1}}$. The detection was questioned because no feature at this velocity was known in the line profiles of other molecules.

In 1984, Anders Winnberg at Onsala Space Observatory in Sweden, performed observations of OH/IR stars with the VLA, with 13 telescopes and baselines ranging from 0.1 to 6.9 km at 1612 MHz. The angular resolution was $7''.5 \times 5''.5$, and the velocity resolution was 1.4 $\mathrm{km\,s^{-1}}$ (Winnberg et al. (1985)).

A preliminary study of the Winnberg (1985) data by Sandqvist revealed a great potential for an extensive mapping with the VLA of OH absorption at the GC, which is the background and basis for this thesis project. The GC is seen at low declinations at the VLA site, about 8 degrees over the horizon, and to achieve a nearly circular beam we concluded that a hybrid array would be preferred.

Subsequently, we submitted a proposal to the NRAO to observe the GC with the VLA in its BnA (former A/B) configuration at the OH main and satellite lines at 18 cm, at the frequencies of 1665, 1667, 1612 and 1720 MHz. In the same period Whiteoak & Gardner wanted to investigate the 132 $\mathrm{km\,s^{-1}}$ emission feature at 1720 MHz further, by observations with higher angular resolution and proposed observations at 1720 MHz with the VLA in the same observation period as ours. The NRAO program committee suggested that the two groups would get the observation time together and share the data, which was accepted by both groups.

The first interpretation of our 1667 MHz observations revealed a feature that later was called the OH-streamer and was published by Sandqvist et al. (1987) and (1989) and further discussed in Karlsson et al. (2003) (Paper I). In Paper I, we also identified the 132 $\mathrm{km\,s^{-1}}$ emission feature as a maser source in the CND, and we used it for a dynamical calculation of the enclosed mass inside a radius of 1.84 pc from the GC. After a comprehensive inspection of the data, we realised the need for complementary observations with the VLA in a more compact array, since there were indications of spurious emission, probably caused by the missing short baselines in the first observational data. We, therefore, proposed for a second observation run with the VLA in the DnC (previously known as C/D configuration) compact array, both for improving the coverage of short baselines and to study larger-scale structures at the GC. The improvement in $(u,v)$ coverage between the BnA and DnC observations is clearly seen in Figs. 3.3 and 3.4. The proposal was granted, and together with the previous VLA observations we logged a total VLA observing time of 24 hours at 18 cm.

Based on the results from the VLA observations, we also decided to use previously unpublished $\mathrm{C^{18}O}$ $J = 2-1$ data of the GC observed with the SEST, as a complement to the VLA data. The SEST data were gathered by Sandqvist in about 100 hours during 1997 and 1999 and are presented in Paper II.

Furthermore, the *Odin* satellite has been invoked in astronomical observations of the GC since 2002, with a total observation time of more than 2000 hours, mainly in the search for water and oxygen. In Paper II, we have included *Odin* observations of water, carbon monoxide, ammonia and neutral carbon at the GC, and water observations were also used in Paper III.

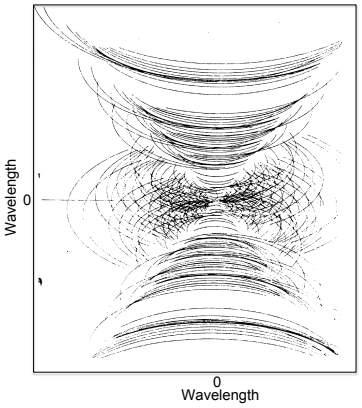


**Figure 3.3:** $(u,v)$ coverage of the VLA BnA observations.

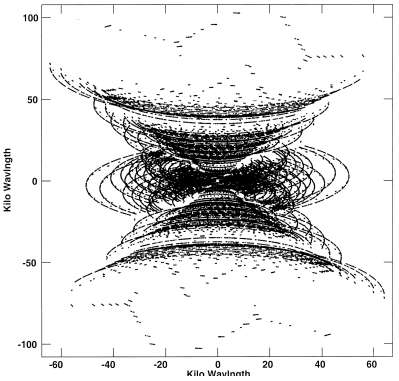


**Figure 3.4:** $(u,v)$ coverage of the DnC observations.

### 3.3.1 VLA observations at 18 cm

#### BnA wide array configuration

The array was centred a few arcseconds off the strongest source (Sgr A*) to avoid interference. In the first observation run, 18 antennas and 64 velocity channels were employed, with a bandwidth of 3.125 MHz. The longest baseline was about 18 km, and the number of baselines was 153. Observations at 18 cm (L-band) yields a primary beam, essentially the field of view, of about 30 arcminutes, and a synthesized beam, angular resolution, of about $4'' \times 3''$. The observations cover a region of about $10' \times 10'$ about Sgr A*.

Absolute flux calibration was made on the Seyfert galaxy 3C286, and as bandpass and phase calibrator the compact non-thermal source of B1748-253 was used. An integration time of 30 s was used for the calibrators and 120 s for the sources. The data were on-line Hanning-smoothed during the observations. Hanning smoothing is used to reduce the so-called Gibbs phenomenon and is a running average across three spectral channels. The Gibbs phenomenon arises when an intrinsically square or sawtooth wave is approximated by sinusoidal waves. By Hanning smoothing, the centre channel is weighted by 0.5, and the surrounding channels by 0.25. Unfortunately, the spectral resolution is somewhat reduced after Hanning smoothing.

The CLEAN algorithm (Högbom (1974)) is a seminal method to interpolate between blank areas in the $(u,v)$-plane and to reduce noise in radio astronomical observations. Variants of CLEAN are invoked in other programs such as in the AIPS program packages of APCLN, IMAGR and MX. Other methods for deconvolution are, however, also available, such as AIPS VTESS, which selects the solution of the observed data having the greatest entropy by

the maximum entropy method (MEM, AIPS Cookbook). In Paper I, we used the VTESS algorithm while we used the AIPS MX and IMAGR program packages in Papers II and III.

Continuum subtraction for the 1665 and 1667 MHz lines in Paper I was made in the map plane using AIPS IMLIN, with a linear fit over feature-free channels in the low and high-velocity wings, for the two respective frequencies of the spectrum. Four line-free channels on the negative velocity side of the 1665 MHz line, and four on the positive velocity side of the 1667 MHz line were averaged and used as continuum map, and the resulting map was used for self-calibration of the data. Noise reduction of those maps was made both with the AIPS APCLN algorithm, and the maximum entropy algorithm (AIPS VTESS program package), with similar results. However, the VTESS was faster and produced maps of a slightly higher quality and was used for the maps in Paper I.

The continuum subtraction for the 1612 and 1720 MHz maps was made from the visibility data in UVLIN in the AIPS program package, and self-calibration of amplitudes and phases were made by the use of a strong maser source. 48 channel maps were produced with a velocity range between $-200$ and 200 $\mathrm{km\,s^{-1}}$. AIPS APCLN was used for noise reduction and compared to that of VTESS, and the difference was found to be insignificant, such that VTESS was preferred even for these maps. The first maps, presented in Sandqvist et al. (1987) (Fig. 3.5), were cleaned by Dr. Jan Högbom using 25 iterations with his experimental program package, Bildprogram för Finsmakare (BIFF), and are of remarkably high quality.

**DnC compact array configuration**

In this observation run, all 27 antennas were employed, and baseline lengths were between 350 m and 1 km. As prime flux calibrator 3C286 was again used for both frequencies and B1751-253 was employed as local flux phase calibrator. The source 1833-210 was used as phase calibrator for both frequencies for 15 minutes at the end of the observations. On-source times were 25 - 30 minutes in each cycle. The data were automatically flagged for shadowing and crosstalk between antennas. A 5 seconds AIPS QUACK was made globally, i.e. a cut of data at the beginning of each period to flag visibilities of low amplitude at the beginning of a scan.

**Concatenation of BnA and DnC data**

To reduce the effects of missing zero- and short baselines in the BnA observations, the BnA and DnC data cubes were concatenated into one data set. The concatenation was performed by the courtesy of M. Goss, and the concatenated

data cube is used in Papers II and III. The angular resolution of those maps is 7” $\times$ 5”, and about 7” $\times$ 7” in the spectral line profiles.

For the production of a continuum map, line-free channels of the concatenated 1665 and 1667 MHz data, respectively, were averaged and subtracted in the $(u, v)$-plane by the AIPS program package UVLIN. The two continuum maps were averaged and used as a continuum for both the 1665 and 1667 MHz data. The resulting spectral line maps were cleaned by about 3000 iterations with the AIPS MX-programme and natural weighting of the data. The typical rms noise in the spectral line maps is about 25 mJy/beam.

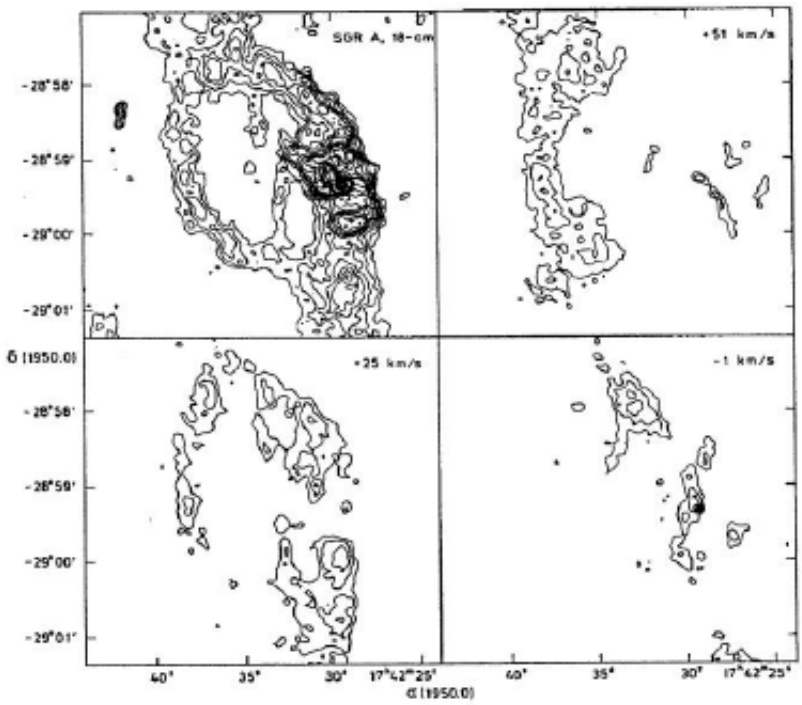


**Figure 3.5:** OH spectral line absorption at 1667 MHz (Sandqvist et al. (1987)), between $-1$ and 51 km s$^{-1}$. The OH-streamer is clearly seen at 51 km s$^{-1}$. The continuum map at 18 cm is shown in the upper left panel, and Sgr A* is located at (R.A, Dec) = ($17^{\rm h}42^{\rm m}29^{\rm s}.30$, $-28^\circ59'.18$”) B1950.0. (Reproduced with permission by The American Institute of Physics).

### 3.3.2 SEST observations at 1.3 mm

The $C^{18}O$ $J = 2 - 1$ observations, at 1.3 mm (219.6 GHz), were carried out in August 1997 and August 1999, towards the Sgr A complex. The observational grid spacing was $22''.5$, and the velocity resolution was 1.0 km s$^{-1}$. The ON-source integration time was 10 minutes per point, at more than 180 positions. The observation grid was selected for compatibility with the 1990-1993 observations of $C^{18}O$ $J = 1 - 0$, by Lindqvist et al. (1995).

The half-power beamwidth of the telescope was $24''$ and the main beam efficiency ($\eta_{\rm mb}$) was 0.60. The dual channel 115/230 GHz superconductor-insulator-superconductor (SIS) on the telescope receiver was used, and the system temperature at the observed frequency of 219.6 GHz was about 250 K most of the time (but could range between 200 and 400 K, depending upon the weather and elevation). The position-switching method was used with the line-free OFF-position at Galactic coordinates $(l, b) = (5', 30')$, see Karlsson et al. (2013), Paper II).

About 180 spectra were sampled in a region of about $10'$ around Sgr A* and were placed on a grid (Fig. A.1 in Paper II). The integrated velocity interval was about +/− 200 km s$^{-1}$. The +50 and +20 km s$^{-1}$ clouds were seen partly, as well as the MB in the SEST observations. The compact H II regions E of the +50 km s$^{-1}$ cloud and several of the previously known maser sources were also identified in Fig. 11 of Karlsson et al. (2013), Paper II.

### 3.3.3 *Odin* observations at submm

The *Odin* satellite was used to map the Sgr A complex at submillimetre wavelengths during 2002-2014. The species studied were $H_2O$, $H_2^{18}O$, $NH_3$, CO, and C I. The telescope was pointed at nine positions in the Sgr A complex. Those positions are indicated in Fig. 1 in Karlsson et al. (2013) (Paper II), by circles whose diameter represents the $2'.1$-beam of the 557 GHz $H_2^{16}O$ observations. The velocity resolution was 0.5 – 3 km s$^{-1}$. The total-power position-switching method and a duty cycle of 120 s were used for most of the observations, with a spectral-line-free region as the OFF-position. The C I observations were performed in the Dicke sky-switching mode that implies a beam-switching against one of two sky horns with a beamwidth of 4.4 degrees, displaced 42 degrees from the main beam (Frisk et al. (2003)).

We observed emission and absorption features at the nine positions, including the +50 km s$^{-1}$ cloud, the CND, the +20 km s$^{-1}$ cloud, the EMR near and far side, high negative gas, the spiral arm features; Local/Sgr arm, the −30 km s$^{-1}$ arm, and the 3-kpc arm.

# 4. Summary of Papers

One of the main results of this thesis are the discovery of the OH-streamer in OH absorption towards the continuum emission at 18 cm at the GC. Moreover, we discuss its relation to the +80 $\mathrm{km\,s^{-1}}$ cloud, the CND, the +20 $\mathrm{km\,s^{-1}}$ cloud, and possibly with the SMBH and the surrounding star cluster, or with an anticipated accretion disk around the SMBH. This work also includes an estimation of the mass inside of 1.84 pc from Sgr A*: nine new maser sources at 1720 MHz: observation of all four previously known compact H II regions on the E side of the +50 $\mathrm{km\,s^{-1}}$ cloud in OH absorption: a possible link between the CND southwest lobe and the EMR: and detection of unusually high abundance of water in shock regions of the CND.

## 4.1 Paper I: 18-cm VLA observations of OH towards the Galactic Centre

Karlsson, R., Sjouwerman, L. O., Sandqvist, Aa., & Whiteoak, J. B. 2003, A&A, 403, 1011(Reproduced with permission ©ESO)

This paper reports on the OH distribution in the Sgr A complex as observed in the 1612, 1665, 1667 and 1720 MHz transitions with the VLA in its BnA configuration. OH absorption maps are presented for the main and satellite transition lines with an angular resolution of $4'' \times 3''$, and a velocity resolution of about 9 $\mathrm{km\,s^{-1}}$. OH absorption was detected towards the +20 and +50 $\mathrm{km\,s^{-1}}$ clouds, the CND, the OH-streamer, and the east and west parts of the Sgr A East shell, as well as towards the HNVG, and the EMR. No OH absorption was observed against Sgr A West, the compact H II regions A-D located E of Sgr A East, or against Sgr A*. Point-like OH emission was detected at all four frequencies. A few point-like maser sources were detected at 1665 and 1667 MHz while a greater number of was observed at the satellite line frequencies of which nine were new detections.

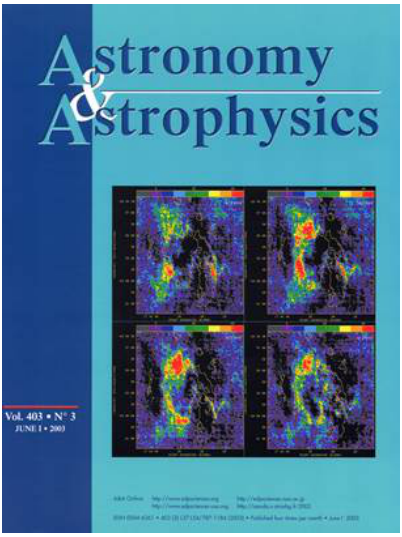


**Figure 4.1:** Front cover of A&A Vol. 403, No 3, June 1, 2003, where Paper I was published, showing OH absorption at 1667 MHz against the GC (Reproduced with permission ©ESO).

## 4.2 Paper II: Hydroxyl, water, ammonia, carbon monoxide, and neutral carbon towards the Sagittarius A complex. VLA, *Odin*, and SEST observations

Karlsson, R., Sandqvist, Aa., Hjalmarson, Å., Winnberg, A., Fathi, K., Frisk, U., Olberg, M., 2013, A&A, 554, A141(Reproduced with permission ©ESO)

In Paper II, we used the concatenated 1665 and 1667 MHz OH VLA BnA and DnC data to minimise the previous concern about missing zero and short baselines in the VLA BnA data. The angular resolution was slightly reduced by the concatenation. Moreover, in this paper, we used unpublished data taken with the SEST telescope and a series of observations with the *Odin* orbital observatory. The *Odin* observations provided us with a long time series of water data and a limited amount of ammonia, neutral carbon and carbon monoxide data.

Besides the OH absorption data, we included observations of $C^{18}O$ $J = 2-1$ emission: $H_2O$ and $H_2^{18}O$ emission and absorption lines: $NH_3$ absorption: C I emission, CO $J = 5-4$ emission in a selection of objects in the Sgr

A complex. The main objects discussed in this paper are the +20, +50 $\mathrm{km\,s^{-1}}$ clouds, the CND and the foreground spiral arm features: the Local/Sgr arm: the $-$ 30 $\mathrm{km\,s^{-1}}$ arm: the 3-kpc arm, the four compact H II regions, and the EMR. For those objects, we present column densities, abundances and comparisons between selected species. We also observed a feature in OH absorption centred at $-32$ $\mathrm{km\,s^{-1}}$ and about 107 $\mathrm{km\,s^{-1}}$ wide at all nine positions that were observed by *Odin*, which we relate to the blue-shifted emission observed in $C^{18}O$ by Genzel et al. (1990).

The SEST $C^{18}O$ data revealed intensity gradients on the western edge of the +50 $\mathrm{km\,s^{-1}}$ cloud adjacent to the four compact H II regions in the + 50 $\mathrm{km\,s^{-1}}$ cloud, and on the southwestern edge of the Sgr A East shell indicating the existence of shock fronts in those regions. A plot of previously known 1720 MHz maser sources onto our $C^{18}O$ emission map (Fig. 11) appears to support our arguments about shock regions where objects seem to interact. The declining velocity gradient from the +50 $\mathrm{km\,s^{-1}}$ cloud, via the molecular belt, to the +20 $\mathrm{km\,s^{-1}}$ cloud is also very clear in the $C^{18}O$ data. Furthermore, we suggest that the SNR (G359.92$-$0.09) is interacting with the molecular belt and the +20 $\mathrm{km\,s^{-1}}$ cloud. In $C^{18}O$ emission, the +20 $\mathrm{km\,s^{-1}}$ or rather the north tip of this cloud (the Southern streamer), appears in projection to bend sharply towards the southwest lobe of the CND, thus supporting ideas of interaction between those objects. In the compact H II region D, we note a two component structure, which may indicate a large scale outflow from the compact H II source D. In the 3-kpc arm we observed a $40''$ diameter ($\sim$ 1 pc) bubble like structure in the emission intensity.

## 4.3 Paper III: The OH-streamer in Sagittarius A revisited: analysis of hydroxyl absorption within 10 pc from the Galactic centre

Karlsson, R., Sandqvist, Aa., Fathi, K., & Martín, S. 2015, A&A, 582, A118 (Reproduced with permission ©ESO)

In Paper III, we present an analysis of certain features in our concatenated data of VLA BnA and DnC observations of 1665 and 1667 MHz OH absorption towards the Sgr A complex at the GC. Our investigation of the properties and kinematics of the OH-streamer and the +80 $\mathrm{km\,s^{-1}}$ cloud in OH absorption indicates that the OH-streamer is an object inside of the CND. Moreover, we argue that the Mid part interacts with the +80 $\mathrm{km\,s^{-1}}$ cloud, the Tail with the CND, and the Head possibly with the strong gravitational field of the SMBH and the surrounding star cluster. We also find indications for interac-

tion between the +80 $\mathrm{km\,s^{-1}}$ cloud or a detached clump of it, and the NE lobe of the CND via the CND NE extension.

We interpret those kinematical and morphological links as indications that gas clumps were disrupted from the SW lobe of the CND, and may have produced the OH-streamer and the +80 $\mathrm{km\,s^{-1}}$ cloud. At least, the OH-streamer seems to be feeding material radially inwards, inside of the CND and towards the GC. For the +80 $\mathrm{km\,s^{-1}}$ cloud, the kinematics are still not resolved. Although the map position of this cloud may suggest that it is a part of the CND, the position-velocity diagrams clearly dispute this.

Moreover, a detailed analysis of the position-velocity diagrams reveals a possible link between the near side of the EMR and the CND SW lobe. In this analysis, we also found OH absorption against all four of the compact H II Regions A-D, East of Sgr A East, both in the 1665 and 1667 MHz transitions.

# 5. Outlook

The kinematics in the OH-streamer Head and its relation to the SMBH, or at least to an anticipated accretion disk at the centre, are not solved. The observations of the Head surrounding the position of Sgr A* and the wing-like structure of the OH absorption there, that seemingly displays an anti-clockwise rotation are tantalising facts worthwhile to probe at higher resolutions. For that purpose, we need observations of both higher angular and velocity resolutions. Moreover, the CN emission observed in the Head calls for further investigation in high resolution data from great facilities such as ALMA.

The location and interactions of the +80 $\mathrm{km\,s^{-1}}$ cloud need to be explained further since we have found possible interactions both in the southwest and northeast parts of the CND.

The new results that the four compact H II regions on the east edge of the +50 $\mathrm{km\,s^{-1}}$ cloud are all at least partly embedded in that cloud, reopen the questions of the origin of those regions and the disagreements in the literature about the age of Sgr A East.

The observation in our OH absorption data of a possible connection between the near side of the EMR and the southwest part of the CND is interesting. If this observation is consistent for other species, it will add to arguments on large- and small-scale coupling of kinematics in the Galaxy, and transfer of material from the bar structure into the GC.

An extended search for 1720 MHz masers in the suggested interaction regions of the OH-streamer, the +80 $\mathrm{km\,s^{-1}}$ cloud, the CND and the EMR would also be interesting to conduct.

A state of the art 3D-presentation and modelling of our observational data of the GC region would be a possible means to shed more light on the morphology and interactions of the observed objects.

# References


Amo-Baladron, M.A., Martín-Pintado, J. & Martín, S. 2011, A&A, 526, 54 32

Baganoff, F. K., Maeda, Y., Morris, M., et al. 2003, ApJ, 591, 891 47

Balick, B., & Brown, R. L. 1974, ApJ, 194, 265 46

Bally, J., Stark, A. A., Wilson, R. W., & Henkel, C. 1987, ApJS, 65, 13 26

Bally, J., Stark, A. A., Wilson, R. W., & Henkel, C. 1988, ApJ, 324, 223 26

Bally, J. 1989, ESOC, 33, 1 23, 29

Becklin, E. E., Gatley, I., & Werner, M. W. 1982, ApJ, 258, 135 32

Binney, J., Gerhard, O. E., Stark, A. A., Bally, J., & Uchida, K. I. 1991, MNRAS, 252, 210 27

Brown, R. L., & Liszt, H. S. 1984, ARA&A, 22, 223 28

Bradford, C. M., Stacey, G. J., Nikola, T., et al. 2005, ApJ, 623, 866 35

Cabrera-Lavers, A., Garzón, F., Hammersley, B., et al. 2006, A&A, 453, 371 22

Chan, M. H., & Ehrlich, R. 2014, Ap&SS, 349, 407 22

Chatzopoulos, S., Fritz, T. K., Gerhard, O., et al. 2015, MNRAS, 447, 948 48

Christopher, M. H., Scoville, N. Z., Stolovy, S. R., & Yun, Min S. 2005, ApJ 622, 346 32, 34

Chuss, D. T., Davidson, J. A., Dotson, J. L., et al. 2003, ApJ, 599, 1116 26

Churchwell, E., Babler, B. L., Meade, M. R., et al. 2009, PASP, 121, 213 17

Coil, A. L., Ho, P. T. P. 1999, ApJ, 513, 752 34, 35

Cuadra, J., Nayakshin, S., Springel, V., et al. 2005, MNRAS, 360L, 55 18, 47

Cuadra, J., Nayakshin, S., Springel, V., et al. 2006, MNRAS, 366, 358 18

Dame, T. M., Hartmann, Dap, & Thaddeus, P. 2001, ApJ, 547, 792 28

Davidson, J. A., Werner, M. W., Wu, X., et al. 1992, ApJ, 387, 189 32, 34, 35

de Vaucouleurs, G. 1964, IAUS, 20, 195 21

Eckart, A., & Genzel, R. 1997, MNRAS 284, 576 48

Eckart, A., Genzel, R., & Ott, T. 2001, IAUS, 205, 20 48

Eisenhauer, F., Perrin, G., Rabien, S., et al. 2005, AN, 326, 561 48

Ekers, R. D., van Gorkom, J. H., Schwarz, U. J., & Goss, W. M. 1983, A&A, 122, 143 30, 39, 44

Ferrière, K. 2012, A&A, 540, A50 28, 39, 40

Frisk, U., Hagström, M., Ala-Laurinaho, J., et al. 2003, A&A, 402, 27 58

Gatley, I., Jones, T. J., Hyland, A. R., et al. 1986, MNRAS, 222, 299 32

Genzel, R., Stacey, G. J., Harris, A. I., et al. 1990, ApJ, 356, 160 38, 61

Genzel, R., Hollenbach, D., & Townes, C. H. 1994, RPPh, 57, 417 28

Genzel, R., Poglitsch, A. 1995, ASPC, 73, 447 25, 34

Genzel, R., Eckart, A., Ott, T., & Eisenhauer, F. 1997, MNRAS, 291, 219 48

Genzel, R., Schödel, R., Ott, T., et al. 2003, ApJ, 594, 812 48

Gerhard, O. 2008, Mem. S.A.It., Vol. 00, 183 21

Ghez, A. M., Klein, B. L., Morris, M., & Becklin, E. E. 1998, ApJ, 509, 678 48

Ghez, A. M., Morris, M., & Becklin, E. E. 1999, ASPC, 182, 24 48

Ghez, A. M., Morris, M., Becklin, E. E., et al. 2000, Nature, 407, 349 48

Gillessen, S., Eisenhauer, F., Trippe, S., et al. 2009, ApJ, 692, 1075 18, 37, 48

Glass, I. S., Catchpole, R. M., & Whitelock, P. A. 1987, MNRAS, 227, 373 39

Goss, W. M., Schwarz, U. J., van Gorkom, J. H., & Ekers, R. D. 1985, MNRAS, 215P, 69 44

Güsten, R., & Downes, D. 1980, A&A, 87, 6 40

Güsten, R., Walmsley, C. M., & Pauls, T. 1981, A&A, 103, 197 38, 46

Güsten, R., Genzel, R., Wright, M.C.H., et al. 1987 ApJ, 318, 124 32, 33, 35, 43

Herrnstein, R. M. H., & Ho, P. T. P. 2005, ApJ, 620, 287 30, 31

Hildebrand, R. H., Davidson, J. A., Dotson, J., et al. 1993, ApJ, 417, 565 34

Högbom, J. A. 1974, A&AS,15, 417 55

Ho, P. T. P., Jackson, J. M., Barrett, A. H., & Armstrong, J. T. 1985, ApJ, 288, 575 38

Ho, P. T. P., Luis C., Szczepanski, J. C., et al. 1991, Nature, 350, 309 40

Hüttemeister, S., Wilson, T. L., Bania, T. M., & Martín-Pintado, J. 1993, A&A, 280, 255 35

Jackson, J. M., Geis, N., Genzel, R., et al. 1993, ApJ, 402, 173 25, 32, 33, 34, 35, 43, 44

Kaifu, N., Kato, T., & Iguchi, T. 1972, NPhS, 238, 105 26

Kaifu, N., Iguchi, T., & Kato, T. 1974, PASJ, 26, 117 26

Karlsson, R., Sjouwerman, L. O., Sandqvist, Aa., & Whiteoak, J. B. 2003, A&A, 403, 1011 32, 34, 35, 38, 39, 40, 46, 48, 49, 54

Karlsson, R., Sandqvist, Aa., Hjalmarson, Å et al. 2013, A&A, 554, A141 32, 35, 38, 39, 40, 45, 58

Karlsson, R., Sandqvist, Aa., Fathi, K., & Martín, S. 2015, A&A, 582, A118 31, 32, 34, 35, 38, 39, 40, 41, 42, 43

Khokhlov, A., Melia, F. 1996, ApJ, 457, L61 31

Kassim, N. E., Larosa, T. N., Lazio, T. J. W. & Hyman, S. D. 1999, ASPC, 186, 403 24

Killeen, N. E. B., Lo, K. Y., & Crutcher, R. 1992, ApJ, 385, 585 29, 40, 43

Latvakoski, H. M., Stacey, G. J., Gull, G. E., & Hayward, T. L. 1999, ApJ, 511, 761 32

Lau, R. M., Herter, T. L., Morris, M. R., et al. 2013, ApJ, 775:37 33, 36

Lindqvist, M., Sandqvist, Aa., Winnberg, A., Johansson, L.E.B., & Nyman, L.-Å 1995, A&AS, 113, 257 58

Liszt, H. S., & Burton, W. B. 1980, ApJ, 236, 779 21

Liszt, H. S., Burton, W. B., & van der Hulst, J. M. 1985, A&A,142, 237 32, 33

Lo, K. Y., & Claussen, M. J. 1983, Nature, 306, 647 37

Maeda, Y., Baganoff, F. K., Feigelson, E. D., et al. 2002, ApJ, 570, 671 30, 35

Marshall, J., Lasenby, A. N., & Harris, A. I. 1995, MNRAS, 277, 594 43

Mapelli, M., & Gualandris, A. 2016, LNP, 905, 205 48, 49

Marr, J. M., Wright, M. C. H., & Backer, D. C. 1993, ApJ, 411, 667 33

Martín, S., Martín-Pintado, J., Montero-Castaño, M., et al. 2012, A&A 539, A29 40, 43

Martinez-Valpuesta, I., & Gerhard, O. 2012, EPJ Web of Conferences 19, 06010 25

McGary, R. S., Coil, A. L., & Ho, P. T. P. 2001, ApJ, 559, 326 34, 35

McMillan, P. J. 2011, MNRAS, 414, 2446 18

Melia, F., Coker, R. F., & Yusef-Zadeh, F. 1996, ApJ, 460, L33 36

Melia, F., & Falcke, H. 2001, ARA&A, 39, 309 29

Meyer, L., Ghez, A. M., Schödel, R., et al. 2012, 338, 84 48

Mezger, P. G., Zylka, R., Salter, C. J., et al. 1989, A&A, 209, 337 38

Mezger, P. G., Duschl, W. J., & Zylka, R. 1996, A&ARv, 7, 289 28, 29

Mills, E., Morris, M. R., Lang, C. C., et al. 2011, ApJ, 735, 84 44, 45

Mo, H. J., Mao, S., & White, S. D. M. 1998, MNRAS, 295, 319 19

Morris, M., Polish, N., Zuckerman, B., & Kaifu, N. 1983, AJ, 88, 1228 25

Morris, M., & Yusef-Zadeh, F. 1985, ApJ, 90, 2511 29

Morris, M., & Serabyn, E. 1996, ARA&A, 34, 645 19, 21, 24, 25, 27, 28, 29, 34, 37

Morris, M., Design Reference Mission Case Study Stratospheric Observatory for Infrared Astronomy Science Steering Committee 201025

Nidever, D., Majewski, S. R., Burton, W. B., et al. 2010, ApJ, 723, 1618 19, 20

Nishiyama, S., Nagata, T., Baba, D., et al. 2005, ApJ, 621, L105 22

Novak, G., Dotson, J. L., Dowell, C. D., et al. 2000, ApJ, 529, 241 34

Okumura, S. K, Ishiguro, M., Fomalont, E. B., et al. 1991, ApJ, 378, 127 35, 38

Paumard, T., Maillard, J.-P., & Morris, M. 2004, A&A, 426, 81 37

Pedlar, A., Anantharamaiah, K. R., Ekers, R. D., et al. 1989, ApJ, 342, 769 38

Peters III, W. L. 1975, ApJ, 195, 617 21

Philipp, S., Zylka, R., Mezger, P. G., et al. 1999, A&A, 348, 768 29

Requena-Torres, M. A., Martín-Pintado, J., Rodríguez-Franco, A., et al. 2006, A&A, 455, 971 25

Quillen, A. C., & Minchev, I. 2005, AJ, 130, 576 22

Roberts, D. A., & Goss, W. M. 1993, ApJS, 86, 133 37

Roberts, D. A., Yusef-Zzadeh, F., & Goss, W. M. 1996, ApJ, 459, 627 36

Rockefeller, G., Fryer, C. L., Baganoff, F. K., et al. 2005, ApJ, 635L, 141 35

Rodríguez-Fernandez, N. J., Martín-Pintado, J. 2001, ESASP, 460, 491 23

Rodríguez-Fernandez, N. J., Martín-Pintado, J., Fuente, A., et al. 2004, A&A, 427, 217 25, 35

Sandqvist, Aa. 1970, AJ, 75, 135 53

Sandqvist, Aa. 1973, A&AS, 9, 391 53

Sandqvist, Aa. 1974, A&A, 33, 413 S 32, 53

Sandqvist, Aa., Wootten, A., & Loren, R. B. 1985, A&A, 152, L25 32

Sandqvist, Aa., Karlsson, R., Whiteoak, J. B., et al. 1987, AIPC, 155, 95 40, 43, 54, 56, 57

Sandqvist, Aa. 1989, A&A, 223, 293 38

Sandqvist, Aa., Karlsson, R., & Whiteoak, J. B. 1989, IAU Symp 136, 421: ed. M. Morris (Kluwer, Dordrecht) 54

Sandqvist, Aa., Larsson, B., Hjalmarson, Å., et al. 2015, A&A, 584, A118 53

Sanders, R. H. 1998, MNRAS, 294, 35 50

Schödel, R., Ott, T., Genzel, R., Hofmann, R., et al. 2002, Nature, 419, 694 48

Schlegel, D. J., Finkbeiner, D. P., & Davis, M. 1998, ApJ, 500, 525 23

Scoville, N. Z. 1972, ApJ 175L, 127 26

Serabyn, E., & Lacy, J. H. 1985, ApJ, 293, 445 44

Serabyn, E., Lacy, J. H., & Achtermann, J. M. 1992, ApJ, 395, 166 44

Shlosman, I. 2012, arXiv:1212.1463 [astro-ph.CO] 21

Sjouwerman, L. O., Pihlström, Y. M., & Fish, V. L. 2010, ApJ, 710L, 111 25

Sofue, Y. 1995, PASJ, 47, 551 27

Sofue, Y., Tutui, Y., Honma, M., et al. 1999, ApJ, 523,136

Sofue, Y. 2011, PASJ, 63, 813 22

Telesco, C. M., Davidson, J. A., & Werner, M. W. 1996, ApJ, 56, 541 34, 35

Tanaka, K., Oka, T., Matsumura, S., et al. 2011, ApJ, 743L, 39 35

Vollmer, B., & Duschl, W. J. 2002, A&A, 388, 128 35

Wegg, C., Gerhard, O., & Portail, M. 2015, MNRAS, 450, 4050 r

Whiteoak, J. B., & Gardner, F. F. 1975, MNRAS, 173P, 25 22

Whiteoak, J. B., & Gardner, F. F. 1976, MNRAS, 174, 627 53

White, G. J. 1996, ASPC, 102, 171 53

Winnberg, A., Baud, B., Matthews, H. E., et al. 1985, ApJ, 291L, 45 33

Yusef-Zadeh, F., Morris, M., & Chance, D. 1984, Nature, 310, 557 32, 53, 54

Yusef-Zadeh, F., & Morris, M. 1987, ApJ, 320, 545 26

Yusef-Zadeh, F., Lasenby, A., & Marshall, J. 1993, ApJ, 410L, 27 46

Yusef-Zadeh, F., Roberts, D. A., Goss, W. M., et al. 1996, ApJ, 466L, 25 46

Yusef-Zadeh, F., Stolovy, S. R., Burton, M., et al. 2001, ApJ, 560, 749 34

Yusef-Zadeh, F., Lacy, J. H., Wardle, M., et al. 2010, ApJ, 725, 1429 32

Yusef-Zadeh, F., Arendt, R., Bushouse, H., & et al. 2012, ApJ 758L, 11 44, 45

Zhao, J.-H., Goss, W. M., & Ho, P. T. P. 1995, ApJ, 450, 122 40

Zhao, J.-H., Morris, M. R., Goss, W. M., & An, T. 2009, ApJ, 699, 186 46

Zylka, R., Mezger, P. G., & Wink, J. E. 1990, A&A, 234, 133 37, 38

Zylka, R., Güsten, R., Philipp, S., et al. 1999, ASPC, 186, 415 38, 39

# Acknowledgements

First, I would like to express the sincere thanks to my supervisor from the beginning, Aage Sandqvist, and his later service as my co-supervisor. Aage has been extremely patient and encouraging during my long periods of a detour for work in other fields. Also, Per-Olof Lindblad has been my distinguished teacher and mentor from the very beginning, and guided me into Astronomy. Great thanks also to Kambiz Fathi for taking over as my supervisor after Aage's "retirement". Kambiz has brought in some of his knowledge and experience in kinematics and dynamics into my work. Kambiz is also very easy to cooperate with, and can make things going in a pleasant way. My thanks also go to Claes Fransson, who has been my mentor. Unfortunately, we did not have much of cooperation before, so I very much appreciate Claes' acceptance to be my mentor.

I am also grateful to the Stockholm Observatory, Department of Astronomy at Stockholm University, for the years I have spent here.

The cooperation with Åke Hjalmarson and Anders Winnberg in preparing Paper II was very fruitful, and Åke brought "overnight delivery" to it's true meaning. Sergio Gelato has been of great and swift help to install and maintain the dear NRAO Astronomical Imaging Processing System (AIPS), which was a necessary element for most of the data reduction. Gustav Taxén and Henrik Edlund at KTH helped me with prototypes for visualisation of the molecular clouds at the GC, a nice work that I hope will be further developed. Hans-Gustav Florén at the Department has been involved in discussions about modelling, and I also hope for a continuation of that project.

Thanks also to Göran Olofsson for his valuable thoughts and hints about the interstellar medium. The often spontaneous discussions with Gösta Gahm were widening my perspective and always very enjoyable. My thanks also go to Lena Olofsson, and Sandra Åberg for their quick support on the administrative side. It was also a great joy to share office room with Torsten Elfhag in the early days, and later with Margaretha Malmort.

Among all the courses I have taken, I would like to mention the inventor of the seminal image processing algorithm CLEAN, Jan Högbom, as one of the best lecturers. His very pedagogic and humble approach to the realm of the Fourier space and image processing has kept on echoing in my head ever since. Jan Högbom's experimental program packages, BIFF (Bildprogram För Finsmakare) and the JHBILD, have put me on solid ground and understanding for the vast amount of image processing in this work. The computing power and storage capacity has improved tremendously at the Department over the years, and I could hardly have managed to complete this work without the processing power of the recent decade. Processing of a quarter size an image could take up to 45 minutes when the first VLA observations were taken, compared to less than a second for a full-size image with today's technology.

Please forgive me all of you who are not dedicated here, but remember I had a very good time at the Stockholm Observatory, and it was all my pleasure.

During the years, my beloved wife Marianne has been my greatest supporter and has taken all her time and care to bring love and welfare to our children and me.